Naval Research Laboratory

Stennis Space Center, MS 39529-5004

NRL/MR/7320--16-9676

On Wave–Ice Interaction in the Arctic Marginal Ice Zone: Dispersion, Attenuation, and Ice Response

Clarence O. Collins III

ASEE Postdoctoral Fellow
Ocean Dynamics and Prediction Branch
Oceanography Division

W. Erick Rogers

Ocean Dynamics and Prediction Branch
Oceanography Division

Aleksey Marchenko

The University Center in Svalbard
Longyearbyen, Norway

June 1, 2016

REPORT DOCUMENTATION PAGE

Form Approved
OMB No. 0704-0188

1. REPORT DATE *(DD-MM-YYYY)*	**2. REPORT TYPE**	**3. DATES COVERED** *(From - To)*
01-06-2016	Memorandum Report	

4. TITLE AND SUBTITLE

On Wave–Ice Interaction in the Arctic Marginal Ice Zone: Dispersion, Attenuation, and Ice Response

5a. CONTRACT NUMBER

5b. GRANT NUMBER

5c. PROGRAM ELEMENT NUMBER
0601153N

6. AUTHOR(S)

Clarence O. Collins III,[1] W. Erick Rogers, and Aleksey Marchenko[2]

5d. PROJECT NUMBER

5e. TASK NUMBER

5f. WORK UNIT NUMBER
73-5097-56-5

7. PERFORMING ORGANIZATION NAME(S) AND ADDRESS(ES)

Naval Research Laboratory
Oceanography Division
Stennis Space Center, MS 39529-5004

8. PERFORMING ORGANIZATION REPORT NUMBER

NRL/MR/7320--16-9676

9. SPONSORING / MONITORING AGENCY NAME(S) AND ADDRESS(ES)

Office of Naval Research
One Liberty Center
875 North Randolph Street, Suite 1425
Arlington, VA 22203-1995

10. SPONSOR / MONITOR'S ACRONYM(S)

ONR

11. SPONSOR / MONITOR'S REPORT NUMBER(S)

12. DISTRIBUTION / AVAILABILITY STATEMENT

Approved for public release; distribution is unlimited.

13. SUPPLEMENTARY NOTES

[1]ASEE Postdoctoral Fellow in the Oceanography Division, NRL
[2]The University Center in Svalbard, Longyearbyen, Norway

14. ABSTRACT

Ice is extremely variable, and because waves and ice may interact in a number of ways depending on the ice and wave characteristics, wave prediction in ice-covered waters is a difficult, and in some ways intractable, problem. A review of wave–ice interaction is made, and special attention is given to formulations of the dispersion relation. The dispersion relation determines the wave attenuation for non-conservative dissipation schemes and contributes to a change of wave height (and direction) analogous to shoaling and refraction. A method for jointly measuring dispersion and attenuation in ice is proposed and it is hoped that two ongoing Office of Naval Research (ONR) Departmental Research Initiatives will provide an opportunity to test and evaluate models of dispersion in ice. In terms of wave effects on ice, a number of new primitive ice models have been recently developed; these are summarized, but much research is needed towards understanding the mechanical properties of ice. Also, additional analysis of wave attenuation during a high wave/ice breakup is presented as a companion for Collins et al. [2015].

15. SUBJECT TERMS

Wave–ice interaction
Dispersion
Attenuation
Marginal ice zone
Floe size distribution

16. SECURITY CLASSIFICATION OF:			**17. LIMITATION OF ABSTRACT**	**18. NUMBER OF PAGES**	**19a. NAME OF RESPONSIBLE PERSON**
a. REPORT	**b. ABSTRACT**	**c. THIS PAGE**			W. Erick Rogers
Unclassified Unlimited	Unclassified Unlimited	Unclassified Unlimited	Unclassified Unlimited	63	**19b. TELEPHONE NUMBER** *(include area code)* (228) 688-4727

.

TABLE OF CONTENTS

TABLE OF FIGURES ..... **iv**

TABLE OF TABLES ..... **v**

EXECUTIVE SUMMARY **E-1**

1 INTRODUCTION 1

1.1 THE MARGINAL ICE ZONE 1

1.1.1 WIND-GENERATED SURFACE GRAVITY WAVES *2*

1.1.2 SEA ICE *3*

1.2 HISTORICAL NOTE 4

2 REVIEW 7

2.1 ICE EFFECTS ON WAVES 7

2.1.1 INTERACTION MECHANISMS *7*

2.1.2 ATTENUATION *10*

2.1.3 DISPERSION RELATIONSHIP IN ICE *11*

2.1.4 REFRACTION AND SHOALING *25*

2.2 WAVE EFFECTS ON ICE 26

2.2.1 OVERVIEW *26*

2.2.2 MODELING ICE *27*

2.2.3 FLOE SIZE DISTRIBUTION *28*

2.2.4 PRIMITIVE WAVE-ICE INTERACTION MODELS *29*

2.2.5 ICE RESPONSE *32*

2.2.6 ADVECTION *33*

2.3 FEEDBACK 33

3 WAVE EVENT 35

3.1 SVALBARD 2010 35

3.1.1 SPECULATIVE FRACTURE INVESTIGATION (A. MARCHENKO) *35*

3.1.2 POST FRACTURE ATTENUATION RATES *36*

4 SPECULATIONS AND CONCLUSIONS 40

4.1 LARGE WAVE EVENTS 40

4.2 WAVES AS A SOURCE OF HEAT? 41

4.3 FINAL THOUGHTS 41

ACKNOLEDGMENTS 42

APPEDDIX A: BENDING AND DISPERSION OF VISCOELASTIC WAVES (MARCHENKO) 43

A.1 BENDING MOMENT IN ICE PLATE WITH ELASTIC AND CREEP RHEOLOGICAL PROPERTIES 43

A.2 DISPERSION EQUATION FOR THE WAVES PROPAGATING IN IDEAL FLUID BENEATH AN ICE PLATE WITH ELASTIC AND CREEP PROPERTIES 46

APPENDEX B: WAVE HEIGHTS MEASURED IN ARTIC ICE 47

REFERENCES 50

TABLE OF FIGURES

FIGURE 1 IMAGE OF THE MIZ WITH HYPOTHETICAL MEASUREMENT POINTS AT VARIOUS LENGTHS STARTING AT THE OPEN SEA EDGE. 10

FIGURE 2 THE NORMALIZED DISPERSION RELATION CALCULATED FROM THE MASS LOADING MODEL AS A FUNCTION OF ICE THICKNESS, H. THE THICKNESS RANGES FROM 0.001 TO 3.500 METERS LINEARLY (ΔH = 0.035 M) WHERE H = 0 IS THE DEEP WATER LINEAR DISPERSION RELATION SHOWN BY THE DOTTED BLACK LINE AND H = 3.5 METERS IS THE DARK RED LINE. 13

FIGURE 3 THE NORMALIZED DISPERSION RELATIONSHIP IN ICE WITH MASS LOADING AND FLEXURAL BENDING OVER 11 DECADES OF SHEAR MODULUS. ICE THICKNESS OF 0.01 M, 0.1 M, 0.5 M, 1.0 M, 2.0 M, AND 3.5 M ARE SHOWN FROM LEFT TO RIGHT, TOP TO BOTTOM. THE SHEAR MODULUS RANGES FROM 1 PA (DARK BLUE) TO 10^{10} PA (DARK RED) WITH LOGARITHMIC SPACING. 15

FIGURE 4 CHANGE IN NORMALIZED WAVENUMBER AS A FUNCTION OF SHEAR MODULUS, G, IN THE FS MODEL. THE COLORS INDICATE ICE THICKNESS AS INDICATED IN THE LEGEND. 16

FIGURE 5 SHOWING THE NORMALIZED DISPERSION RELATION ON THE LEFT AND THE CORRESPONDING ATTENUATION COEFFICIENT ON THE RIGHT. FROM TOP TO BOTTOM THE ICE THICKNESS IS 0.1, 0.5, 1.0, AND 3.5 M. THE COLORS INDICATE THE VISCOSITY RANGING OVER 5 DECADES. THE DISPERSION RELATION DOES NOT CHANGE AS A FUNCTION OF VISCOSITY, THEREFORE ALL LINES ARE OVER PLOTTED AND THE ONLY VISIBLE LINE IS DARK RED (LAST ONE PLOTTED) AND THE BLACK DOTTED LINE IS THE OPEN WATER RELATION. 19

FIGURE 6 LEFT SIDE: DISPERSION RELATION ACCORDING TO THE EXTENDED FOX AND SQUIRE MODEL. THE COLOR INDICATES ICE THICKNESS, H. SHEAR MODULUS IS SET TO THE VALUE 10^5 AND VISCOUS PARAMETER TO THE VALUE 0.01. THE MASS LOADING MODEL (ML) AND PURELY ELASTIC MODEL (FS) ARE SHOWN WITH THE BLACK DOTTED LINE AND BLACK DASHED LINED, RESPECTIVELY. RIGHT SIDE: ATTENUATION COEFFICIENT CORRESPONDS TO THE LEFT SIDE. 20

FIGURE 7 REPRODUCED FROM FIGURE 4 A. OF LUND ET AL. [2015] (COPYRIGHT AMERICAN METEOROLOGICAL SOCIETY) SEE THE REFERENCE FOR FULL DETAILS. CROSS-SECTION THROUGH THE 3D IMAGE SPECTRUM IN THE PEAK WAVE DIRECTION. WAVENUMBER ON THE X-AXIS AND ANGULAR FREQUENCY ON THE Y-AXIS. "STILL WATER" REPRESENTS THE OPEN WATER, LINEAR DISPERSION RELATION (WITHOUT CURRENT) SHOWN BY A SOLID BLACK LINE. THE COLOR CODE (BLUE TO RED) INDICATES THE ENERGY DETECTED BY MR. A SPEED OF 0.52 MS^{-1} PRODUCES A GOOD FIT (BLACK DASHED LINE) TO THE DISPERSION CURVE MEASURED BY THE RADAR (ENERGY SIGNIFICANTLY ABOVE THE BACKGROUND NOISE LEVEL). HIGHER ORDER HARMONICS ARE DETECTABLE IN THE MR SPECTRUM. 23

FIGURE 8 SPECTRAL EVOLUTION OVER THE COURSE OF FIVE HOURS. THE BLACK LINE IS THE SWAN "NO ICE" REFERENCE. THE COLORED SPECTRA ARE CALCULATED FROM THE SEA SURFACE ELEVATION SIGNAL FROM R/V LANCE AND MOVE FORWARD IN TIME FROM DARK BLUE TO GREEN. 36

FIGURE 9 THE SPECTRAL ATTENUATION RATES AS A FUNCTION OF WAVE PERIOD. THE LIGHT COLORED LINES ARE THE INDIVIDUAL CALCULATIONS AND THE BLACK LINE IS THEIR MEAN. THE DOTTED LINE IS THE EMPIRICAL MODEL FROM MEYLAN ET AL. [2014]. 37

FIGURE 10 MAP SHOWING SOUTHERN TIP OF SVALBARD, NORWAY INCLUDING HOPEN ISLAND (ALL MARKED IN GREEN). THE ICE CONCENTRATION IS A PRODUCT OF THE PIPS MODEL AND GIVEN BY THE COLORED CONTOURS WITH THE WHITE INDICATING THE 75 % CONCENTRATION CONTOUR. THE SHIP TRACK IS MARKED IN COLOR AND THE DISTANCES TO THE 75 % CONTOUR ARE GIVEN PARALLEL TO THE DOMINANT WAVE DIRECTION AS GIVEN BY WW3 AND REPRESENTED BY Z_1, Z_2, Z_3, AND Z_4. 38

FIGURE 11 SAME AS FIGURE 9 WITH THE ADDITION OF COLORED DASHED LINES REPRESENTING THE MEAN ATTENUATION RATES USING SWAN. THE COLORS BLUE, GREEN, AND CYAN REPRESENT SCALING OF 1, 2, AND 4, RESPECTIVELY. 39

FIGURE A-1. ICE PLATE FLOATING ON THE WATER SURFACE. 42

TABLE OF TABLES

TABLE 1 SUMMARY OF PRIMITIVE WAVE-ICE INTERACTION AND FSD MODELS..... 32
TABLE 2 SUMMARY OF THE PUBLISHED ACCOUNTS OF WAVES MEASURED IN ICE IN THE ARCTIC REGION... 48
TABLE 3 SUMMARY OF THE PUBLISHED ACCOUNTS OF WAVES MEASURED IN ICE IN THE ANTARCTIC REGION. 49

EXECUTIVE SUMMARY

Ice is extremely variable, and because waves and ice may interact in a number of ways depending on the ice and wave characteristics, wave prediction in ice covered waters is a difficult, and in some ways intractable, problem. A review of wave-ice interaction is made, and special attention is given to formulations of the dispersion relation. The dispersion relation determines the wave attenuation for non-conservative dissipation schemes and contributes to a change of wave height (and direction) analogous to shoaling and refraction. A method for jointly measuring dispersion and attenuation in ice is proposed and it is hoped that two ongoing ONR Departmental Research Initiatives will provide an opportunity to test and evaluate models of dispersion in ice. In terms wave effects on ice, a number of new primitive ice models have been recently developed, these are summarized, but much research is needed towards understanding the mechanical properties of ice. Also, additional analysis of wave attenuation during a high wave/ice breakup is presented as a companion for Collins et al. [2015].

1 INTRODUCTION

This document is concerned with the interaction of wind-generated sea surface gravity waves (henceforth waves) with sea ice. The physics of wave-ice interaction is equally applicable in both of the Polar Regions, although the oceanography of the Arctic, the exclusive location of the recent Office of Naval Research (ONR) sponsored field work and the focus of this report, is quite distinct from the Antarctic. In simple terms, the Arctic is ocean surrounded by land and the Antarctic is land surrounded by ocean. This difference in geography plays a role in ice extent as a result of wave action: the Arctic is mostly ice-covered in the winter so fetch, and hence wave action, develops primarily in warmer summer months. Waves may facture the ice which increases the lateral surface area, increased surface area accelerates melt for smaller floes. An increased fraction of open water also leads to albedo feedback effects and increased fetch. The increased fetch further increases the potential for the development of more damaging waves. Overall, waves work to reduce the ice in the Arctic, while in the Antarctic the most energetic waves occur in the winter at which point ice fracturing may contribute to increasing the ice extent. This is because waves are facilitating the outward export of ice as broken floes, with the leads between floes subsequently freezing over during these cold months [Squire and Montiel, 2015].

ONR has sponsored two related Department Research Initiatives (DRI): the Marginal Ice Zone Program and the Sea State and Boundary Layer Physics of the Emerging Arctic Ocean (Sea State) [Thomson et al., 2013]. The purpose of this document is to review the current body of science in anticipation of new results from these DRIs as well as provide documentation of additional analysis of a dataset from the University Center in Svalbard. This document is necessarily limited in scope, for more comprehensive reviews of wave-ice interaction in the MIZ please see chapter 6 of Wadhams [2000], Squire et al. [1995], and Squire [2007]. Parts of section 2.2 have been expanded in an independent manuscript in progress of publication [Collins et al., 2016].

1.1 THE MARGINAL ICE ZONE

Large regions of the Arctic, particularly in the winter months, experience total, compact ice cover (so-called pack ice). In between the ice-free, open seas and the pack ice exists a gradient of ice. This transition zone is the marginal ice zone (MIZ). The MIZ is characterized by ice which weakens in concentration towards the open sea, often with decreasing floe sizes and thicknesses. As the ice concentration increases, so does the ice effect on wave propagation. Deep in the ice pack, wave energy is severely attenuated and therefore wave effects on ice are limited.

As is easily observable with satellite remote sensors (which have been operational since 1978), on the scales of seasons, the MIZ retreats into the interior of the Arctic as ice melts during the summer months reaching a minimum on average in September. The ice extent

Manuscript approved February 10, 2016.

returns during the winter as the Arctic water refreezes. The ice that survived from the previous year is known as “multi-year ice” while new ice is called “first-year ice”. This distinction is important because the mechanical and thermodynamic properties are quite different between the two. On the scale of climate, observations show that more and more multi-year ice is melting (implying decreasing minimum ice extent), and thus the ratio of first-year ice to multi-year ice is on the rise. This has led to the speculation of a possible ice-free Arctic in the future, figuratively and literally opening up a new ocean to the world with “new” natural resources available for exploitation. Already, there is more navigable Arctic Ocean due to the historically low summer ice extents.

Therefore, there is an impetus to better understand the retreat of sea ice including possible connections of scales through feedback loops. Besides the large scales previously mentioned, wave-ice interaction occurs on mesoscales (e.g. MIZ migration during large storms), sub-mesoscales (smaller storms and gales, changes in floe size distribution), and micro-scales (energy fluxes, fracture events). Little is known about the smaller, sub-meso- and micro-scales because of lack of comprehensive observations. The main idea behind the Arctic Sea State DRI is to observe at these scales and integrate the findings into current operational oceanography.

1.1.1 Wind-Generated surface gravity waves

Waves are a ubiquitous and fundamental part of nature. All bodies of water on Earth mediate the propagation of surface waves, and understanding of their physics, dynamics, and interactions is an essential prerequisite for describing the Earth environment and climate system. For many applications, particularly sea-keeping and ocean operations, medium-range forecasts with hourly resolution are sufficient. At these scales, information about the waves is reported in terms of the wave spectrum, i.e. individual waves are treated statistically not deterministically, though the spectrum itself evolves deterministically. So-called third generation (3G) spectral wave models were developed for this forecasting of this class, and their operational implementation have become one of the great success stories of modern geoscience.

1.1.1.1 3G WAVE MODELS

All 3G wave models (e.g. SWAN “Simulating WAves Nearshore” [Booij et al., 1999], WW3 “WAVEWATCH III” [Tolman, 1991; Tolman and the WAVEWATCH III® Development Group, 2014]) are based on the phase-averaged, action balance (also known as radiative transfer) equation:

$$\frac{\mathrm{D}N}{\mathrm{Dt}} = \sum_i \frac{S_i}{\sigma}$$

This describes the conservation of wave action (spectral density divided by frequency) where the material derivate, $\frac{\mathrm{D}}{\mathrm{Dt}}$ - change in time and divergence, balances the sum total of sources and sinks of wave energy, S_i, and σ is the intrinsic, radial wave frequency.

On the open ocean and in deep water, the main source terms are input of energy by wind (S_{in}), dissipation of energy by breaking/white capping (S_{ds}), and redistribution of wave energy through weakly non-linear, wave-wave interactions (S_{nl}) (e.g. Cavaleri et al., 2007). Recent work has focused on refinement of S_{in} and S_{ds} (see Ardhuin et al., 2009, Rogers et al., 2012, and references within), and more realistic implementation of S_{nl} (e.g. Tolman 2013; Rogers and Van Vledder, 2013).

When waves propagate into the MIZ, there is strong a modification of these source terms (though the details are not known). Besides modification of open water source terms, the wave interaction with sea ice necessitates a new source term, S_{ice}. The first implementation of ice effects on waves was a simple partial blocking of energy flux scaled by ice concentration [Tolman, 2003], rather than via physics (S_{ice}). This was recently improved upon by the implementation of physics-based S_{ice} schemes [Doble and Bidlot, 2013; Rogers and Orzech, 2013; Rogers and Zieger, 2014].

1.1.2 Sea Ice

Though somewhat variable, the salinity of oceanic waters differentiates it from its fresh water counterpart by 35 “salt” grams per liter. These salts fundamentally alter the thermodynamics of the water including the freezing/melting point. At this typical salinity (and at the pressure of 1 atmosphere), the freezing point of sea water is -2° C.

The mechanical differences between first- and multi- year ice were previously mentioned. When sea ice forms, the water freezes and the salts are concentrated into brine channels. These brine channels add to the porosity of ice. It turns out that porosity is inversely proportional to the flexural strength, i.e. very porous ice has weak flexural strength. As ice warms in the spring, the network of brine channels may connect and drain out of the ice. If the ice survives the melt season, then it is much less porous after refreezing. In this way multiyear ice possess much more flexural strength and therefore is more resistant to breaking [Timco and Weeks, 2010]. Much of the difficulty in determining the appropriate wave-ice interaction is a result in uncertainty in mechanical ice properties. These properties are difficult (and in some cases impossible) to measure in the field. Various mechanical properties are important to the study of ice – wave interaction including (but not limited to): thickness, density, porosity, salinity, temperature, Young’s modulus, shear modulus, Poisson’s ratio, creep and fatigue properties, and breaking strength. Due to difficulties of in situ measurements of these properties, these are better known for first year ice than for multiyear ice. Even in a small area of first year ice, the mechanical properties may be subject to significant additional dependencies in vertical axis due to

change in temperature and salinity or in time due to creep, fatigue, and eventual failure [Squire and Montiel, 2015].

In addition to first- and multi-year ice solid pack ice, there are many more forms of sea ice forged by interactions with the environment and all of these may be varied and nuanced in nature. The fact that the Inipaiq Eskimos of Wales, Alaska have 120 words for sea ice [Krupnik and Weyapuk Jr, 2010] reflects the many variations of its form in nature. For a review of the properties of sea ice in the Arctic, see Wadhams [1981], and an engineering context see Timco and Weeks [2010].

Since ice is so varied, it is useful to define homogeneity of ice conditions in two ways. If, on the large scale, a particular mechanism of wave-ice interaction is dominant, but the ice characteristics are varied, then this may be thought of as a qualitative large-scale homogeneity. An example would be a large, relative thin ice sheet with a thickness which slowly changes over space. Small-scale homogeneity, by contrast, is more strictly defined. In the previous example, strict (small-scale) homogeneity would imply uniform ice thickness. If multiple regimes of wave-ice interaction are appropriate within the scale of interest (e.g. multiple scattering by individual floes abruptly transitioning to solid pack ice), this violates any sense of homogeneity. Obviously, the appropriateness of the homogeneity assumption will depend on the scales of interest.

1.2 HISTORICAL NOTE

Man has explored frozen waters near or in the Arctic since the time of the Viking Era. In a quest for shorter shipping routes, there were several expeditions into the Arctic Ocean in the 1800s. Ships would become stuck in the sea ice, some relenting under the immense, crushing pressure. The *Fram* was specially built for withstanding this pressure; to survive the grip of the ice and drift along within it. During its maiden voyage (1893-1896) the crew sailed deep into the ice with the intentions of putting *Fram* to this test. During this time the crew managed many to record many scientific soundings (e.g. pressure, depth, location). The first explorers to reach the North and South Pole achieved the feat in 1908 (or possibly 1909) and 1911, respectively.

By the mid-1940s, the Soviets were by far the leaders in Arctic science, having had an almost continuous scientific presence since 1935. Professor N. N. Zubov's book on Arctic ice (which was eventually translated into English) was perhaps the first treatise on the subject [Zubov, 1945].

Many passages in Zubov's book are remarkable; here we reproduce several which are directly related to the interaction of waves and ice:

> The deflection of ice under the weight of a load is ordinarily compared to the problem of deflection of an elastic plate on an elastic foundation. But this problem presupposes uniformity of the plate and ice is extremely heterogeneous, both vertically and horizontally... Finally, when loads are

> moved on ice, the ice deflects in conformity with the "water" wave which forms under it. All these facts taken together create unusual difficulties for a mathematical analysis and make it necessary to have recourse to formulas which even though approximate, still satisfy the practical requirements.

His description of the state of affairs for the treatment of the waves propagating through ice is astonishingly appropriate for modern wave-ice interaction modeling. Since the time of Zubov's book, many analytical problems have been solved with sophisticated treatments of waves propagating through non-uniform ice (e.g. Squire, 2007). However the complex mathematical treatments are not appropriate for application in phase-averaged, spectral wave models which in practice are the workhorses responsible for forecasting waves in the Arctic and thus many simplifications are necessary.

An anecdote, related by Zubov via an earlier publication by Bernstein, might be the first recorded observations of waves under ice cover:

> Observer repeatedly noted the appearance of wind ripples on the thin Ice. Bernstein points out that the instrument observations carried out in 1927 on the Volga established, without a doubt, the origin of the wind fluctuations of the ice level. Thus, with a wind of 13 m/sec. (which corresponds to a pressure of 21 kg/m^2 on a surface perpendicular to the wind), a constant agitation of the Ice (Irregular periods of 20 to 180 sec.) was observed. The amplitude reached 3 mm (figure 86). In calm weather, fluctuations of an equal order were not observed.

The Volga, running through central Russia, is the longest and largest (by discharge) river in Europe. Observations of Arctic ice vibration thought to be connected to wind disturbances were published by Fakidov [1934] where it was noted that vibrations would often precede the oncoming wind. This might be explained by the propagation of flexural-gravity waves which may outrun the storm which generated them.

The Soviet Icebreaker *Gerogy Sedov* was sent to the Arctic in 1929 for a high latitude expedition. In 1937, the *Sedov* became stuck in the ice and was eventually converted into a research station (the first North Pole research station) which spent 812 days drifting in the ice. The captain's log was described in Zubov's book with several fascinating entries which may be the first accounts of wave causing the breakup of Arctic ice:

> On 26 January [1938], a storm set in which lasted six days. The ice field began to undergo more powerful oscillations. The period of these oscillations was 10 to 12 seconds and was the sum of the waves [sic] period and the period of its own fluctuations. The inclination of the ice field reached 60 angular seconds or more. As a result of these oscillations, tensions were generated in the ice field, which finally caused

> it to break up on 1 February along lines approximately perpendicular to the wind direction. A large surge undoubtedly caused these fluctuations and thus the break-up of the ice field. The surge was caused by stormy winds in the neighboring ice-free areas of the Greenland Sea and spread in all directions according to a general law.

Again, according to Zubov:

> On 12 January 1940, it was noted in the log of the Sedov:
>
> '2100, significant surge 30 m - when the ridge passed, ice was raised a little and broke open. When the base of the wave had passed, the ice rejoined with a creak, characteristic of jamming. The phenomenon occurred with a periodicity, characteristic for a heavy sea of 9-10 sec.'

Over the years, seismic or "gravity meter" observations followed which correlated millimeter (or less) movement of the ice with wind or storms [Crary et al., 1952; Hunkins, 1962; LeSchack and Haubrich, 1964].

If the ice floes are much smaller than the wave length of the impending ocean wave, then gravity is still the sole restoring force (though there is additional inertia due to the mass of ice) and these waves are essentially ocean waves modified by the presence of ice. As water waves make their wave into much larger floes (than the wavelength) or solid pack ice, where the model of a large elastic sheet or beam may be appropriate, then they prorogate through the ice as coupled wave modes known as flexural-gravity waves. These flexural-gravity waves may be thought of as "ice waves" as now the restoring force is gravity plus the flexural properties of the ice sheet or beam, in other words, ice is the interfacial medium which supports the waves, and it was these ice waves which were first measured. The first account of ocean waves propagating through the marginal ice zone and ice fields comes from Robin [1963]. Studies postdating these will be referenced in the review below (section 2) and cataloged in the context of wave height in Appendix B.

2 REVIEW

2.1 ICE EFFECTS ON WAVES

As ice is varied in nature, the effect of ice on waves is also varied (e.g. Campbell et al., [2014]). The most documented property is attenuation. Attenuation is the result of many individual mechanisms responsible for dissipating wave energy as waves interact with ice. These mechanisms are typically split into two broad categories: 1) conservative ($S_{ice,c}$) and (2) non-conservative attenuation mechanisms ($S_{ice,nc}$) [Rogers and Zieger, 2014]. In the context of a spectral wave model, $S_{ice,c}$ includes wave scattering and reflection, so although wave energy is attenuated along the main propagation direction into the ice, the energy is being redirected (e.g. backwards toward the open water) rather than dissipated. For $S_{ice,nc}$, waves also attenuate along the main propagation direction, but the wave energy is essentially lost to unresolved dissipation processes. Some losses are caused by differences between local horizontal motion of the ice and water, implying a frictional effect which goes to turbulence and then heat in the water. In the case of ice floes, this friction results in horizontal motion of the ice floes, and if these floes are colliding or ridging, wave energy will be lost to friction and even noise and potential energy. Normal pressures at the water/ice interface, on the other hand do not inherently dissipate wave energy, but if there are energy losses in the ice caused by the vertical motion of the ice (e.g. hysteresis or internal friction), then energy is again lost to heat[1].

In general there are two overarching regimes of interaction. One is when the horizontal extent of the ice floe is large compared to the typical wavelength. In this limit, one may model ice as an elastic sheet, then wave may propagate through the ice as flexural-gravity waves. Dissipation in this regime may be due to formation of turbulent boundary layers beneath the ice. The second is when the horizontal extent of the ice floe is small compared to the typical wavelength. Then the waves are essentially water waves with extra mass loading. Grease ice may damp small waves via viscous interaction of ice particles. Snell's law may be applied to understand change in propagation direction and wave height of the incoming waves in analogy to refraction, and similar for group velocity in analogy to shoaling (more on this in section 2.1.4).

2.1.1 INTERACTION MECHANISMS

2.1.1.1 CONSERVATIVE ATTENUATION: SCATTERING

Scattering is a universal wave process by which waves are deflected by some object. A classic example is the Rutherford's gold foil experiment, where he discovered the atomic nucleus from scattering patterns of alpha particles aimed at the foil. Similarly ocean waves may be scattered by obstacles, including ice. Scattering sends part of the wave energy

[1] One might speculate that this production of heat in the ice could contribute in some small way to melting.

away from the main direction of propagation, so that along the main direction, wave energy is attenuated. If ice is much larger in scale then the incident wavelength, then scattering will important.

A simple ice model is a semi-infinite thin elastic sheet (so called Euler-Bernoulli thin elastic plate [Squire, 2007]). Waves will scatter at the interface, so that some of the energy is transmitted into the ice and some of the energy is reflected back out to sea. As waves propagate through realistic ice, there is scattering due to imperfections (i.e. ridges and sails) and discontinuities (i.e. change in ice thickness, cracks, etc.). Scattering also occurs upon entering and leaving leads and polynya (open water regions in pack ice cover). Scattering may also occur in the interaction with a single floe, and many of these single floe interactions can be synthesized together in a sophisticated way and treated as multiple scatterers. Many complicated mathematical models exist for scattering and the specific problems mentioned above, see [Squire, 2007] for a review.

Typically, to solve the scattering problem, one needs detailed information about the ice floes and wave phases which is never available in practice, so most of this work has not been translated into a form for practical application in 3G wave models. The recent development of primitive wave-ice interaction models [section 2.2.4] has allowed the scattering attenuation based on the number of floes in the domain [Kohout and Meylan, 2008].

2.1.1.2 NON-CONSERVATIVE ATTENUATION: DISSIPATION

Alternative to or in concert with scattering, one may consider non-conservative dissipation. The main mechanisms for non-conservative dissipation are covered in Zhao et al. [2015]:

1. One way to introduce dissipation is through viscosity or internal friction (hysteresis) of the ice. For example modeling the ice layer as a continuum with some finite viscosity, that is, there is a finite ice layer has some rheological properties would be appropriate for frazil type ice. A purely elastic ice layer does not permit this type of dissipation. However viscosity is introduced, it is a two-layer fluid problem, and the viscosity of the ice layer or water layer will leach wave energy. Several rheological models are available in the literature (e.g. Robinson and Palmer [1990], Fox and Squire [1994], and Keller [1998])
2. Another way to dissipate energy is in the viscous sublayer below ice. This type of dissipation is possible even when assuming that the ice is purely elastic (i.e. no viscosity in the ice). Imagine a very large ice sheet, such that the ice does not move horizontally to match the wave induced horizontal velocity. The interaction of the horizontal water motion with a stationary boundary induces a turbulent boundary layer flow directly beneath the ice. The velocity of the particles goes must to zero at some point, depending on the roughness length associated with the underside of the ice. Energy is dissipated in the viscous sublayer close to the ice. This

"turbulence under ice" concept has been used in the sink term formulated by Liu and Mollo-Christensen [1988] and Liu et al. [1991]. It should be kept in mind that their derivation is primarily to predict the dispersion relation for a case of mass-loading with an elastic sheet, and the "turbulence under ice" scheme was added as an afterthought via an eddy viscosity term in order to produce dissipation. It is also a concept used in the physical argument of De Carolis and Desiderio [2002], who again apply it as if the turbulence is a viscosity in the water layer.

3. Consider again an ice floe which is large compared to the wavelengths. As the wave propagates as a flexural-gravity wave, the ice under goes compression and decompression twice per wavelength. This ice will react with some inelasticity, meaning the bending motion alters the mechanical structure of the ice. This is known as elastic hysteresis. Related to this a mechanism for structural failure and eventual breakup of ice. At some number of cyclical loads, N, the ice may facture at stresses lower than the yield stress, a phenomenon known as fatigue. Another related problem is the permanent strain due to sustained stress, known as creep. Creep is an issue closely related to temperature. Wadhams [1973] provides a formulation of the creep problem. Another way to think of these processes is in terms of failure mechanics. Creep is ductile or plastic failure, where the deformation or stretching of the material leads to failure over time. Fatigue is the propagation of small cracks, where the crack length lengthens over time and eventual lead to failure. The creep physics used by Wadhams [1973] were taken from existing knowledge of slow movement of glaciers, so its validity for the rapid cyclical motion of the wave-in-ice problem is not known. On the other hand, the ability of this motion to cause fatigue in the ice is intuitive.
4. Now consider ice floes which are small compared to the wavelengths such that the ice floes more or less respond to the horizontal particle motion. If the floes are densely packed then there will be collisions between floes. There are a number of processes resulting from inelastic collision: the edges of floes are floes may be smashed, grated, pulverized resulting in a slurry, or the floe may crack, break, or raft (pile on top of each other) etc. The permanent changes in ice, including potential energy via rafting, must drain some energy from the wave system. Also, significant noise is may be generated as floes collide, effectively transporting away some energy from the wave system. These effects are of such complexity that they may remain strictly in the realm of phase-resolved and floe-resolved modeling, to be included in WW3-type models only in gross and highly parameterized representations.

One may take lump all of these effects together, in analogy to turbulence closure, into an effective phenomenological viscosity [Liu and Mollo-Christensen, 1988; Wang and Shen, 2010]. The latter intended their model as a continuous (i.e. without switching between models) representation of the ice cover via two variables which are specified independently:

The viscosity property comes from the frazil ice or ice floes much smaller than wavelength. Interaction of these small "particles" and their hydrodynamic interaction with the surrounding water create an effective viscosity for the ice layer. The elasticity property comes from the rigidity of ice floes in which floe sizes are relatively large compared to the wavelength. When the ice is consisted of frazil or small ice floes, a viscous parameterization should be appropriate for the ice cover. When the ice cover is a continuous ice sheet, an elastic parameterization is appropriate.

2.1.2 Attenuation

Introducing dissipative processes into the formulation of the interaction problem may yield direct estimates of attenuation. The difficulty is that various dissipation mechanisms (some with well-defined models, others without) may or may not be appropriate for given conditions. Some require homogenous (even isotropic) conditions, where the MIZ is heterogeneous in general. Many mechanisms may be active at the same time. Apart from dissipation, wind input is still active over ice, although it is thought to be drastically reduced [Bidlot et al., 2014]. There may be normal wave generation in the small fetches of leads and polynya. The sum total of all of these effects are rolled up into the calculation of bulk attenuation of wave energy typically as a function of distance into the ice.

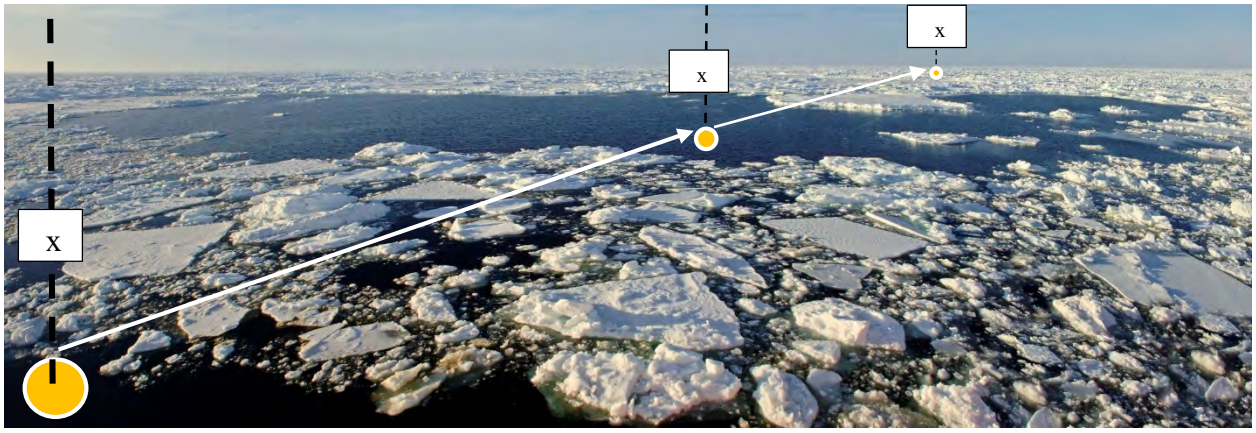

Figure 1 Image of the MIZ with hypothetical measurement points at various lengths starting at the open sea edge.

The solutions to the scattering problem as well as measurements indicate wave energy attenuations exponentially of as a function of distance [Wadhams et al., 1988]:

$$\frac{\partial S_x}{\partial x} = -\alpha S_0 \qquad (1)$$

Here S_0 is the wave frequency spectrum at position x = 0 and α is the attenuation coefficient. This is solved as follows:

$$S_x(f) = S_0(f)\exp(-\alpha x) \tag{2}$$

Imagine the situation as pictured in Figure 1. There are three measurement locations. Starting at the open sea edge at the far left you measure in the incoming wave spectrum, $S_0(f)$. You also have measurements of the wave spectrum at two locations deeper into the MIZ, $S_x(f)$. In this case, Eq. 2 may be inverted to yield the coefficient of attenuation:

$$\alpha(f) = -\frac{\log(S_x/S_0)}{x} \tag{3}$$

Scattering models and non-conservative dissipation models may produce a direct estimate of the attenuation which may be compared to these measurements. However, measuring the attenuation in this way does essentially provides no information on details of dissipation mechanisms (hence the term "bulk property" is sometimes used) and other sources and sinks or wave energy unrelated to, but perhaps strongly modified by, ice may be active. So, it may come to no surprise that it is not a trivial task to compare model estimates of α with measurements nor should measurements be expected to agree under different conditions.

The ideal measurement scenario is to have an unforced swell system that is propagating directly into the ice, normal to a clearly defined ice edge (or floe field boundary), with in situ measurements at several points inside the ice, and one point outside. The measurements should be directional in order to distinguish the effects of scattering vs. dissipation. Of course, a real, in situ measurement effort will be faced with wave and ice conditions that are considerably less "tidy", and so there usually must be some educated guesswork and approximation.

2.1.3 Dispersion Relationship in Ice

Attenuation due to non-conservative mechanisms is inseparable from dispersion, as we shall see. Dispersion refers to the fact that surface waves of different wavelengths and frequencies travel at different speeds, and so "disperse" in space and time. The wavelength and wave frequency are related through a dispersion relationship.

The dispersion relationship is derivable from first principles: conservation of energy and momentum for a fluid element lead to the Navier-Stokes (NS) equation and the continuity equation. Detailed derivations are available in the literature (e.g. Kinsman [1965] or Collins III [2014]). Several assumptions are made about water at this point so that many terms in the NS are negligible. This includes neglecting viscosity (though it is included later as one model of attenuation), compressibility, and assuming water is irrotational. If water is assumed to be incompressible and irrotational, the fluid velocity can be described by the gradient of scalar function called the velocity potential. Without getting very deep into the details, the dynamic boundary conditions at the interface require the normal stress to be continuous and the shear stress to vanish (for inviscid water surface). The

stress-strain relationships are determined by the mechanical model of the ice. These stress-strain relations are then used in the potential flow theory to derive the dispersion relation.

By linearizing the dynamic boundary condition at the surface, the open water (i.e. ice free) dispersion relation is:

$$\omega = \sqrt{gk \tanh kd} \tag{4}$$

For simplicity, we will take this to the deep water limit, such that tanh(*kd*) goes to 1:

$$\omega = \sqrt{gk} \leftrightarrow \frac{\omega^2}{g} = k \equiv k_{ow} \tag{5}$$

We will maintain the deep-water limit throughout the remainder of the text though this can easily be extended to full intermediate water form. Here we define k_{ow} as the open water wavenumber. Complications due to ice are introduced through enforcing extra terms (i.e. due to the added inertia due to the existence of ice on the surface, the bending due to the flexural rigidity, and the compressive stress) in the boundary conditions and then re-deriving the dispersion relation. Details of these derivations can be found throughout the literature (e.g. Squire et al. [1995], Squire [2007], and Wang and Shen [2010]).

2.1.3.1 MASS-LOADING MODEL

The first, and perhaps simplest, way ice effects were introduced is by including the added mass at the interface; this is known as the mass loading model (originally developed by Weitz and Keller [1950]).

$$\frac{\omega^2}{g - \rho_{ice} h \omega^2 / \rho} = k \tag{6}$$

Following Liu and Mollo-Christensen [1988], the presentation can be simplified by defining an inertial coefficient, $M = \rho_{ice} h / \rho$:

$$\frac{\omega^2}{g - M\omega^2} = k \tag{7}$$

The model of added mass is quite general, so specifics of ice are introduced though the inertial coefficient with the inclusion of material density, ρ_{ice}, and thickness, *h*. For producing Figure 2, the density of sea water was set as 1025 kgm^{-3} and ρ_{ice} was 10% less than ρ. There is only one free parameter, *h*, and as the *h* goes to zero, the inertial term in the denominator goes to zero and the relationship simplifies to that of open, deep water relationship of Eq. 5.

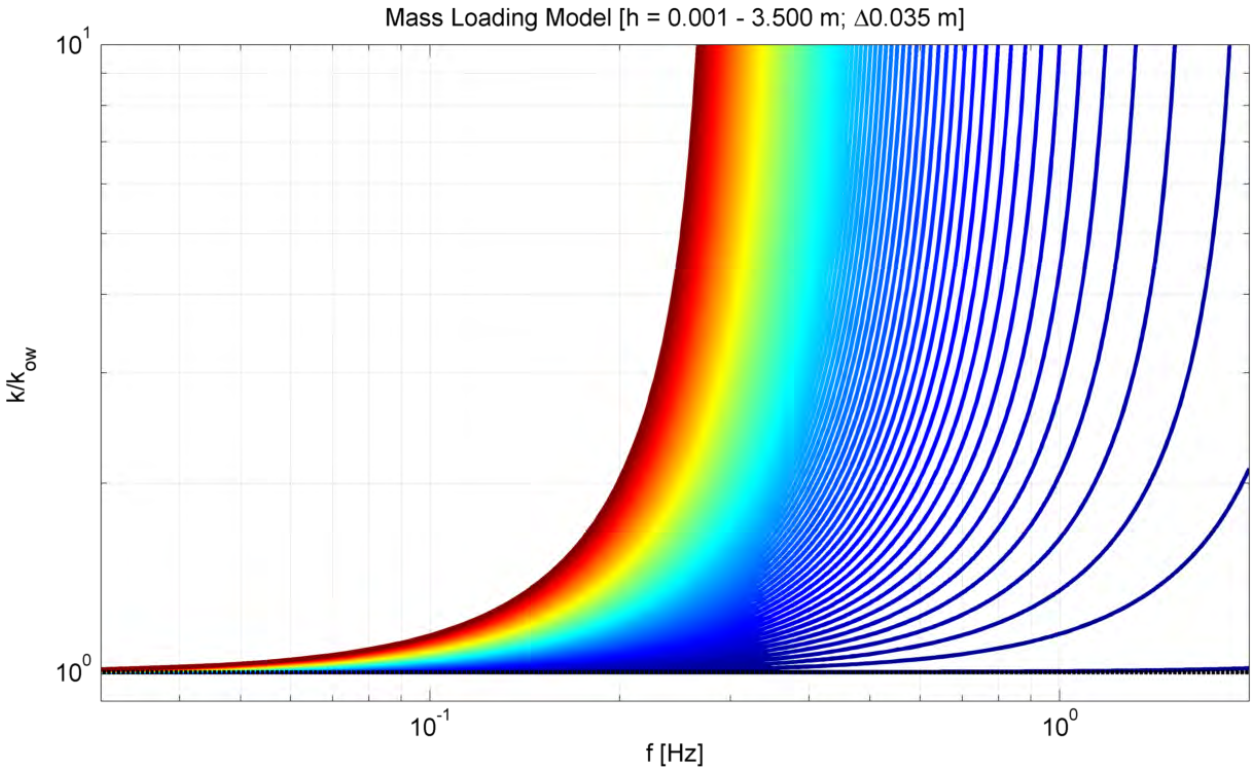

Figure 2 The normalized dispersion relation calculated from the mass loading model as a function of ice thickness, h. The thickness ranges from 0.001 to 3.500 meters linearly (Δh = 0.035 m) where h = 0 is the deep water linear dispersion relation shown by the dotted black line and h = 3.5 meters is the dark red line.

The effects of different thickness ice on the dispersion relation is shown in Figure 2. The wavenumber calculated with the mass loading model is normalized by the open water wavenumber, k_{ow}, so that the y-axis shows the change in wavenumber. Figure 2 shows that mass loading model (1) always increases the wavenumber (shortens the wavelength) and (2) that the change in wavelength is most important for higher frequencies. Even for very thin ice, h = 0.035 m, the wavenumber corresponding to 2 Hz is double that of the open water relationship. For long waves, $f < 0.1$ Hz, the effect mass loading of ice up to 3.5 m thick is not substantial. There is a 15% increase in wave number at 0.1 Hz.

The mass loading model may be appropriate for conditions where the elastic properties of ice are unimportant and floes do not interact with other floes. This would be the case for long waves propagating through small (compared to the wavelength), sparse pancake ice.

2.1.3.2 PURE ELASTIC ICE WITH MASS LOADING

The next level of complexity requires that some assumptions about the mechanical behavior of ice must be made, which determine the stress - strain relationship. In the context of wave-ice interaction, ice may be regarded as an isotropic, homogenous elastic plate (or beam) due to the strain rates in involved. The stress is supplied by the incoming wave field, and the strain describes the response of the ice which, through enforcing the

dynamic boundary conditions must be continuous at the ice – water interface. This is an application of the Euler-Bernoulli beam theory or its extension, Kirchoff-Love plate theory. Conceptually, this might occur when the ice is a large, thin plate which surface waves may induce coupled wave modes. After re-deriving the dispersion relation, the material property of flexural rigidity shows up in the denominator as a term proportional to k^4.

$$\frac{\omega^2}{g - M\omega^2 + Lk^4/\rho} = k \tag{8}$$

Here *L* is the flexural rigidity of the sea ice which is a function of three ice parameters (1) the thickness, *h*, (2) the effective elastic modulus, *E*, and (3) the Poisson ratio, *v*:

$$L = \frac{Eh^3}{12(1 - v^2)} \tag{9}$$

In the purely elastic regime, there exists a simple relationship between the Lamé constants E, ν, and G:

$$E = 2G(1 - v)$$

$$G = E/(2(1 - v))$$

$$v = \frac{E}{2G} - 1$$

So we can easily choose the free parameter to be G. Flexural term in the dispersion relation tends to lengthen the wavelength [Squire, 1993]. The net wavelength, whether shorter or longer, depends on the balance between mass loading and the flexural rigidity. We use the Euler-Bernoulli beam model of Fox and Squire [1994] (FS) to examine a few of the possibilities.

According to Figure 3, whether the wavelength shortens or lengthens depends on the relative contributions of the mass loading and flexural rigidity terms in the denominator. When the shear modulus goes to zero, then the pure mass loading Eq. 6 is recovered from Eq. 8.

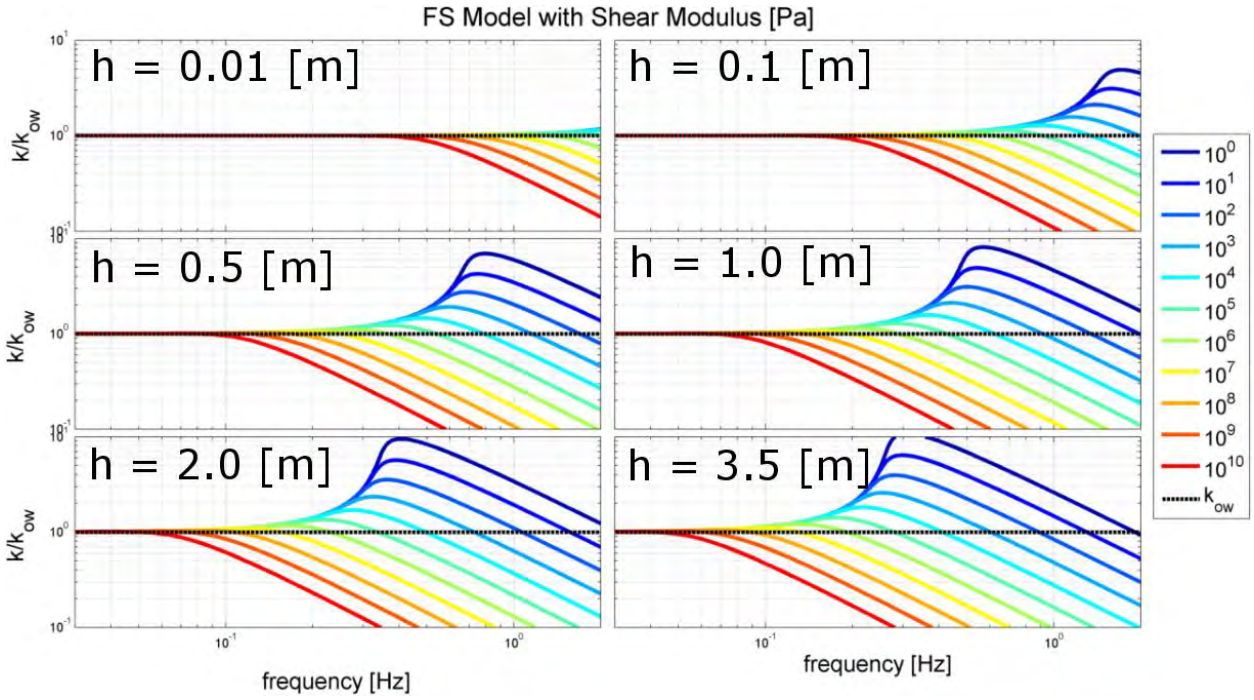

Figure 3 The normalized dispersion relationship in ice with mass loading and flexural bending over 11 decades of shear modulus. Ice thickness of 0.01 m, 0.1 m, 0.5 m, 1.0 m, 2.0 m, and 3.5 m are shown from left to right, top to bottom. The shear modulus ranges from 1 Pa (dark blue) to 10^{10} Pa (dark red) with logarithmic spacing.

If we choose a typical wave frequency, say 0.1 Hz, how does the shear modulus change the wavelength? Figure 4 shows that a 0.1 Hz does not change from the mass loading model, even in thick ice of h = 3.5 m. For the thickness tested, deviations from the mass loading model slowly appear beyond a shear modulus of 10^6 Pa. For a given h, after the effects of flexural appear, the wavelength rapidly increases as a function of G (and h). For the same level of shear modulus, say 10^{10}, a change in ice thickness from 1 m to 2 m leads to a large change in wavelength of ~60 m.

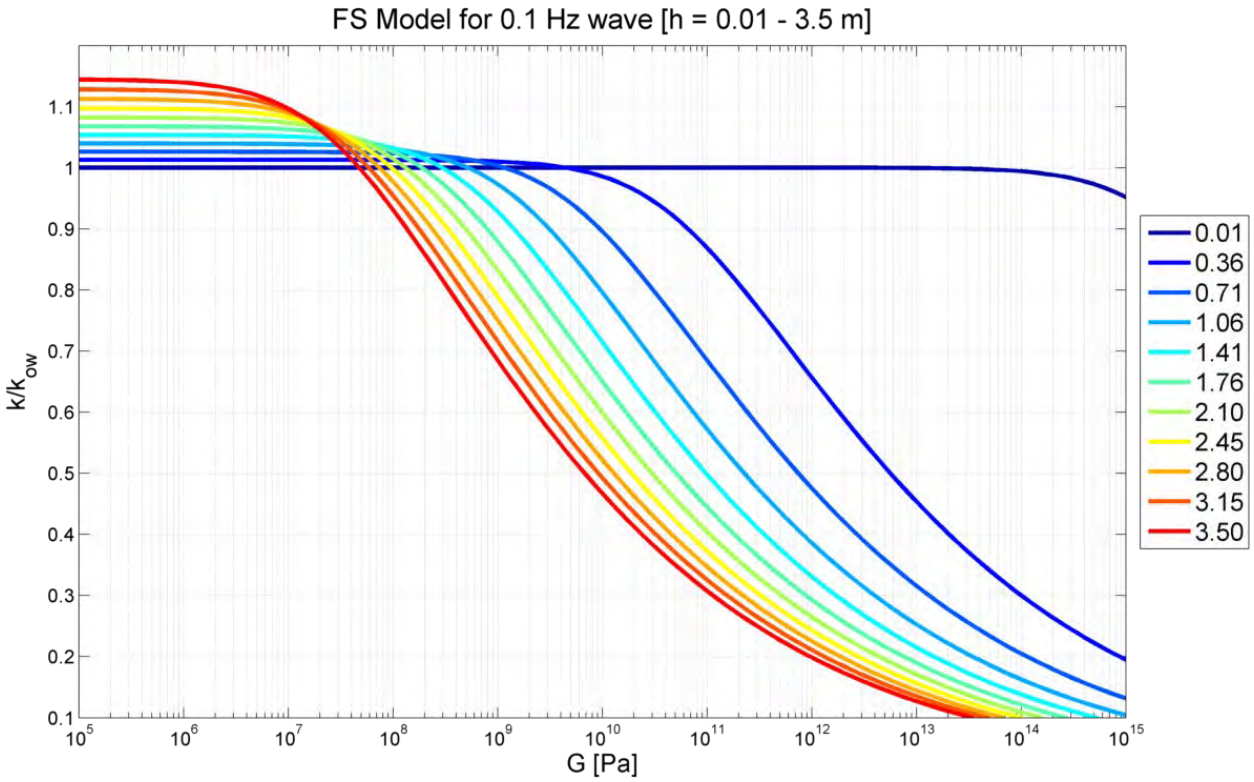

Figure 4 Change in normalized wavenumber as a function of shear modulus, G, in the FS model. The colors indicate ice thickness as indicated in the legend.

Before we move on to dissipative models we should note that the effects of ice compression have also been explored. These are thought to be important in pack ice under high compressive stress [Liu and Mollo-Christensen, 1988].

$$\frac{\omega^2}{g - M\omega^2 + Bk^4 - Phk^2/\rho} = k \qquad (10)$$

Where we have introduced the bending coefficient, $B = L/\rho$, and P is the compressive stress. We can further simplify by defining a compressive coefficient, $Q = Ph/\rho^2$

---

[2]There is an interesting analogy between compressive stress in wave dispersion with the effects of surface tension, the equation for which bears the form:

$$\omega^2 = \left(gk + \frac{\tau k^3}{\rho}\right)\tanh dk$$

Where τ is the surface tension of water. By taking this form to the deep water limit, and rearranging:

$$\frac{\omega^2}{g + \tau k^2/\rho} = k$$

Now, the surface tension, T, and the compressive stress can be related by the following equation:

$$P = -\frac{\tau}{h}$$

So that compressive stress acts as negative surface tension scaled by the ice thickness.

$$\frac{\omega^2}{g - M\omega^2 + Bk^4 - Qk^2} = k \tag{11}$$

The effect of compressive stress is to increase the wavenumber, but the compressive stresses assumed in Liu and Mollo-Christensen [1988] are considered unrealistic under most conditions [Timco and Weeks, 2010] so this formulation has lost favor in the community. This is perhaps most appropriate during a strong on ice storm event in which the ice edge becomes compact due to wave and wind forcing. Recent studies of ice fracture by waves [Asplin et al., 2012; Kohout et al., 2014; Collins et al., 2015; Kohout et al., 2015] insinuate that perhaps this model deserves some renewed attention.

2.1.3.3 VISCOUS AND VISCOELASTIC MODELS

Up until this point, we have not mentioned wave energy. This is because although the previous models changed the wavelength, the wave energy is conserved. In contrast, introducing viscosity, by itself, does not significantly change the wavelength for the viscosities considered here, but it does change the energy as a function of propagation distance.

The formulation of dissipation may be introduced by one of several models. One may introduce a viscoelastic model such as the Voigt model or Maxwell model [Wang and Shen, 2010] which determine the form the deviatoric stress-strain relationships. Different physics are active for different models including a spring-dashpot (damped oscillator) for the Voigt model, viscosity of the water layer or ice layer or both, viscosity proportional to the water velocity (friction), fatigue or creep strain (one such model is derived in Appeddix A: Bending and Dispersion of viscoelastic waves (Marchenko)), and others. A class of these are known as visco-elastic models [Wang and Shen, 2010; Mosig et al., 2015].

To talk about viscous dissipation we need to back up a step and reformulate the dispersion in terms of a complex wavenumber:

$$k = k_0 + i\alpha \tag{12}$$

Assuming the real and imaginary parts are separable[3], solving for the real part of the dispersion relation gives the wavenumber (as in the previous examples) and solving for the imaginary part gives the attenuation coefficient, α. For a monochromatic wave of amplitude A which is a function of distance, x:

$$A(x) = A_0 e^{ikx}$$

Substituting in the complex wavenumber

[3] This is apparently not possible for the model of Wang and Shen [2010] [J. Mosig, personal communication].

$$A(x) = A_0 e^{ix(k_0+i\alpha)} = A_0 e^{-\alpha x} e^{ik_0 x}$$

Here the second term on the right hand side gives the attenuation and the third term is gives the oscillation. Exponential attenuation arises as a natural consequence of the complex wave number, this is known in physics as the evanescent mode. Therefore, attenuation is direct result of solving the dispersion relation. Given the group velocity, $C_g \equiv \frac{\partial \omega}{\partial k}$, the attenuation coefficient may be written in terms of the space or time domain. Giving the attenuation rate as a function of length serves as a convenient implementation of the ice source term [Rogers and Zieger, 2014]:

$$\frac{S_{ice}}{E} = -2C_g\alpha \tag{13}$$

In Eq. 11 (and therefore its limits Eqs. 6 and 8) dissipation has not yet been introduced. In the non-conservative regime, dissipation follows directly from the formulation of the dispersion relation. Visco-elastic models neglect compressive stress but expand on Eq. 8 including an additional imaginary term within the term proportional to k^4.

$$\frac{\omega^2}{g - M\omega^2 + Dk^4} = k \tag{14}$$

Where D has a real part (B from above) and imaginary part consisting of any number of specific complex formulations, one of which we will expand on below. We shall proceed with an example of a viscoelastic model: the extended model of Fox and Squire, [1994] (EFS). This model follows from analogy to a spring-dashpot and introduces a viscosity (or friction) proportional to frequency into the elastic plate model above. The dispersion relationship for EFS is as follows:

$$\frac{\omega^2}{g - M\omega^2 + \frac{G_v h^3}{\rho 6}(1+v)k^4} = k \tag{15}$$

Here G_v is complex Voigt shear modulus [Mosig et al., 2015] which is related to the elastic shear modulus, G, and the viscosity parameter (related to the dashpot-constant), [4]η:

$$G_v = G - i\omega\rho_{ice}\eta \tag{16}$$

So that Eq. 15 can be expanded to

[4]Not to be confused with sea surface elevation for which η is typically used in the literature.

$$\frac{\omega^2}{g - M\omega^2 + Bk^4 - i\omega\rho_{ice}\eta\frac{h^3}{\rho 6}(1+v)k^4} = k \tag{17}$$

Figure 3 was produced by setting η to zero in Eq. 17, therefore reducing the EFS to the FS, and then varying the value of G. With all other parameters staying the same, for the values of viscosity tested, changing viscosity alone does produce a significant change to the real part of the wavenumber and hence does not alter the wavelength (this is verified in [Mosig et al., 2015]). It does however, change the level of attenuation.

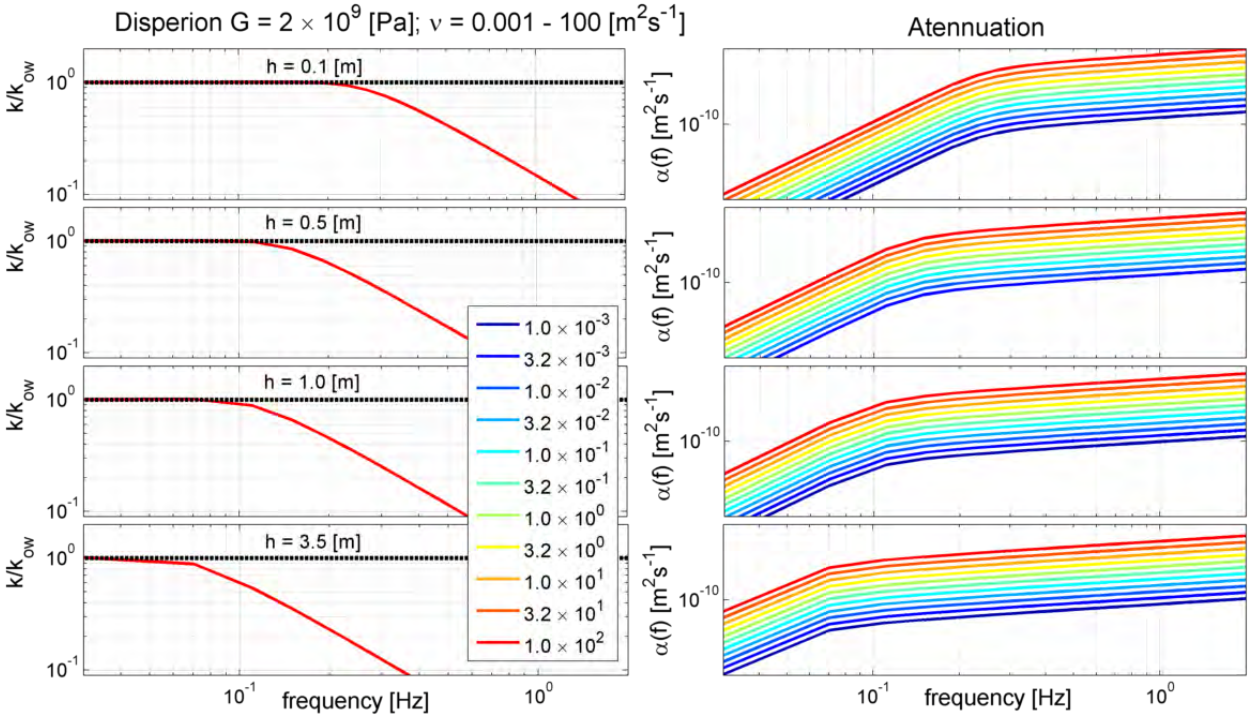

Figure 5 Showing the normalized dispersion relation on the left and the corresponding attenuation coefficient on the right. From top to bottom the ice thickness is 0.1, 0.5, 1.0, and 3.5 m. The colors indicate the viscosity ranging over 5 decades. The dispersion relation does not change as a function of viscosity, therefore all lines are over plotted and the only visible line is dark red (last one plotted) and the black dotted line is the open water relation.

Figure 5 shows the normalized dispersion relation on the left side and on the right the attenuation coefficient. From top to bottom the ice thickness is 0.1, 0.5, 1.0, and 3.5 m, respectively. G is set to 2 x 10^9 to the value used in Doble and Bidlot [2013] and the variation of v is shown with color. Because dispersion is not a function of viscosity in this formulation, all the dispersion curves lie on top of one another, leaving only the most last one plotted (dark red) visible. In contrast, the attenuation rate varies monotonically with viscosity. The change in slope in attenuation space can be seen to correspond with deviation from the open water dispersion relation. Attenuation rates are highest for the high frequencies. Given the same viscosity, whether or not attenuation increases or

decreases with a change in ice thickness depends on the frequency. Comparing the top and bottom plots on the right hand side, the lower frequency (< 0.10 Hz) attenuation is drastically increased and the higher frequency (> 0.30 Hz) attenuation is slightly decreased.

To explore this a bit further, we set reasonable values for elastic shear modulus, G = 10^5, and viscous parameter, η = 0.01. We vary the ice thickness from 0 – 5 m, the value of thickness indicated by color ranging from dark blue to red, respectively. For reference, solution for the dispersion relation with ice thickness of 5 m for the mass loading model (ML) and purely elastic model (FS).

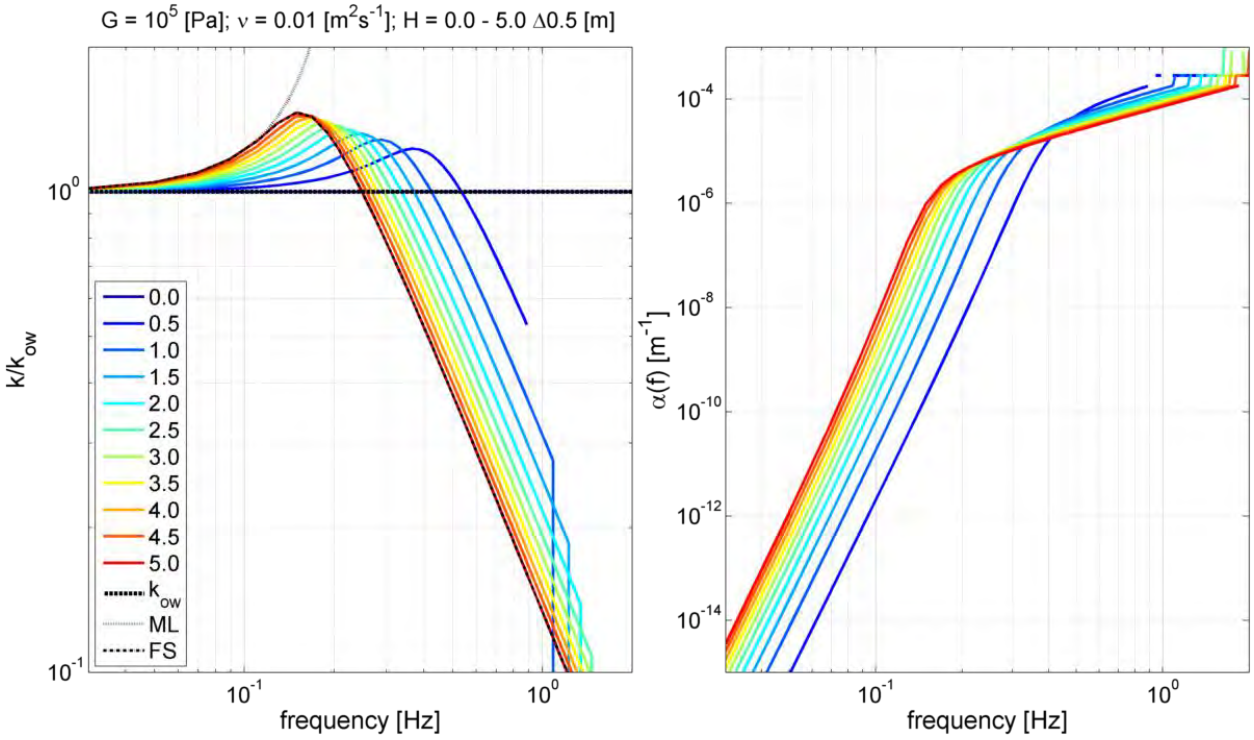

Figure 6 Left side: Dispersion relation according to the extended Fox and Squire model. The color indicates ice thickness, h. Shear modulus is set to the value 10^5 and viscous parameter to the value 0.01. The mass loading model (ML) and purely elastic model (FS) are shown with the black dotted line and black dashed lined, respectively. Right side: Attenuation coefficient corresponds to the left side.

The left of Figure 6 shows the dispersion relation calculated using the EFS model with color showing ice thickness. The solution for h = 5, matches that of the purely elastic model (FS) exactly. All three models (EFS, FS, and ML) give indistinguishable k for frequencies less than 0.15. On right side, attenuation is a function of frequency, with attenuation most important for the high frequencies. The transition in slope for the attenuation corresponds with the dispersion relation transitioning from mass loading dominant to elasticity dominant. Before the transition, the attenuation increased monotonically with thickness, the opposite is true after the transition, resulting in an unintuitive situation: for high frequency (> 0.5 Hz) waves less ice means more attenuation.

That being said, one should keep in mind that relationship being tested is based on Euler-Bernoulli beam theory which valid only for infinitesimal strains. For high frequency waves (> 0.5- Hz), the reflection will be nearly 100% [Fox and Squire, 1995] so a phenomenal amplitude is required to register strain. In essence, such a situation is not physically feasible to begin with.

Lastly there are some artifacts to point out. Where a dispersion relation for a particular thickness appears to drop-off or disappear is an error (correspondingly in attenuation appears step-wise). The solver is giving the wrong root (e.g. see Mosig et al. [2015]) and the parameters involved are outside the validity of the model (personal communication with V. Squire [2015]). Apparently, compared to the model of Wang and Shen [2010], the EFS model is the less susceptible to these sorts of errors and great care needs to be taken to ensure the proper root is chosen (again, see Mosig et al. [2015]). Devising a system for choosing roots of the complex dispersion relation (e.g. Zhao et al. [2015]) is an active area of research.

In the limit that ice is homogeneous, one could specify which dispersion relation is appropriate depending on the ice and wave properties. So the running assumption is an isotropic ice medium. Anisotropies and organized ice patterns will lead to deviations from the derivations below. For large-scale, but not fine-scale homogeneity, different properties of the ice will manifest in the measured dispersion relation. Using an average ice thickness where in reality ice thickness varies would be analogous estimating a vehicle's speed by dividing the distance covered by the travel time, when in reality, for whatever reason (perhaps traffic), the speed of the vehicle was not constant. In this way, one might refer to a measured dispersion relation as a bulk dispersion relation. This being said, the assumption of ice as a continuum may be a gross oversimplification in some cases.

2.1.3.4 DISPERIONS MEASUREMENTS

We have introduced several simple mathematical treatments for dispersion of surface waves in ice, and although equations are somewhat simple to show, the solutions produced are very mathematically rich. The measurements of the dispersion relationship in ice are much fewer than those of attenuation, and hence bulk dispersion relationship is even less well understood than bulk attenuation in practice. The difficulty is that estimation of the dispersion requires spatio-temporal information, e.g. co-located measurements of wave period and wave length. In the end, any measurements of dispersion in ice are a manifestation of many individual mechanisms of wave ice interaction and thus, like attenuation, is bulk property. Whereas the mechanisms described above are predominately dissipative and clearly lead to bulk attenuation, the dispersive outcomes of the individual mechanisms are mixed (could be a balance of mechanisms which increased and decreased wavelength) leading to ambiguous results.

Several studies attempted to use SAR data to measure the dispersion relation [Wadhams and Holt, 1991; Liu et al., 1991]. For the most part, it was found that the wavelength decreased which supported the mass loading model in the case of Wadhams and Holt [1991] and high compression in the case of Liu et al. [1991], though evidence was generally limited in both studies. Fox and Haskell [2001] was able to estimate the propagation speeds of waves (and hence indirectly the wavelength) in ice by measuring the frequency spectrum at two closely located positions. Their Figure 6 shows that fitted empirical wavelength is slightly longer for frequencies within the 0.05 – 0.10 Hz band and then significantly shorter for frequencies from the 0.10 – 0.16 Hz band. Sakai and Hanai [2002] in a lab experiment with synthetic ice, found that the dispersion relationship (between 0.6 and 1.7 Hz) varied between a flexural model and a mass loading model as a function of floe length scale. The transition must have been dependent on the relative scales of the wavelengths and floe sizes so that at any one time the measured dispersion relation is a mixture of the mass loading and flexural-gravity models. The higher frequencies showed the greatest celerity ranges (the range itself a function of ice thickness).

Under very precise laboratory conditions, literally performed on a desk top, both the dispersion relationship and attenuation has been directly measured in viscous water for waves in the gravity-capillary wave range [Behroozi et al., 2010]. By controlling the wave frequency and generating a standing wave, they were able to measure the wavelength (giving dispersion) and the change in wave height with space (attenuation). They were then able to invert the dispersion relation to give an estimate of the viscosity. In the context of field experiments, there are obvious technical challenges which differentiating the two settings: a spectrum, not a single frequency, of waves will be freely propagating, not standing. A standing wave removes the spatial dependence of wave properties, so in the field a spatio-temporal measurement needed, of which there are very few examples and none in ice.

Here we speculate on how to accomplish such a measurement. There are few techniques for spatio-temporal field measurements, one category is stereo-video systems (e.g. Campbell et al. [2014]) and another is ship borne X-band marine radar systems (MR). We concentrate on the latter since MR has recently been utilized in icy conditions as part of the Sea State DRI. MRs transmit microwave pulses and record the backscatter intensity, and backscatter is dominated by the Bragg scattering mechanism [Young et al., 1985; Borge et al., 1999]. The backscatter is tracked in space and time. The time of return provides the radial distance (range) and the look direction of the antenna provides the angle. The rate of rotation can be such that MRs produce one complete (360°) scan of the sea surface nearly every second. One then performs a 3D Fourier transform of the time series snapshots to get a 3D image spectrum and which is then converted to a 2D wavenumber spectrum, details for which may be found in (e.g. Lund et al. [2014]).

The cornerstone to the MR method is a direct measurement of the location of wave energy in 3D Fourier space which is defined by the dispersion relation:

$$\omega = F(k) + \boldsymbol{k} \cdot \mathbf{U}$$

Where F(k) is whatever form of the dispersion relationship is applicable and **U** is the surface current vector. Usually, the dispersion relation for linear, open water is the only applicable dispersion relation, so that deviations from the linear dispersion curve indicate the presence of a current. A wave spectrum under the influence of a uniform surface current experiences a Doppler shift. Therefore, measured deviations from the linear dispersion relation are assumed to be in the form of a current-induced Doppler shift (e.g. Senet et al. [2001]).

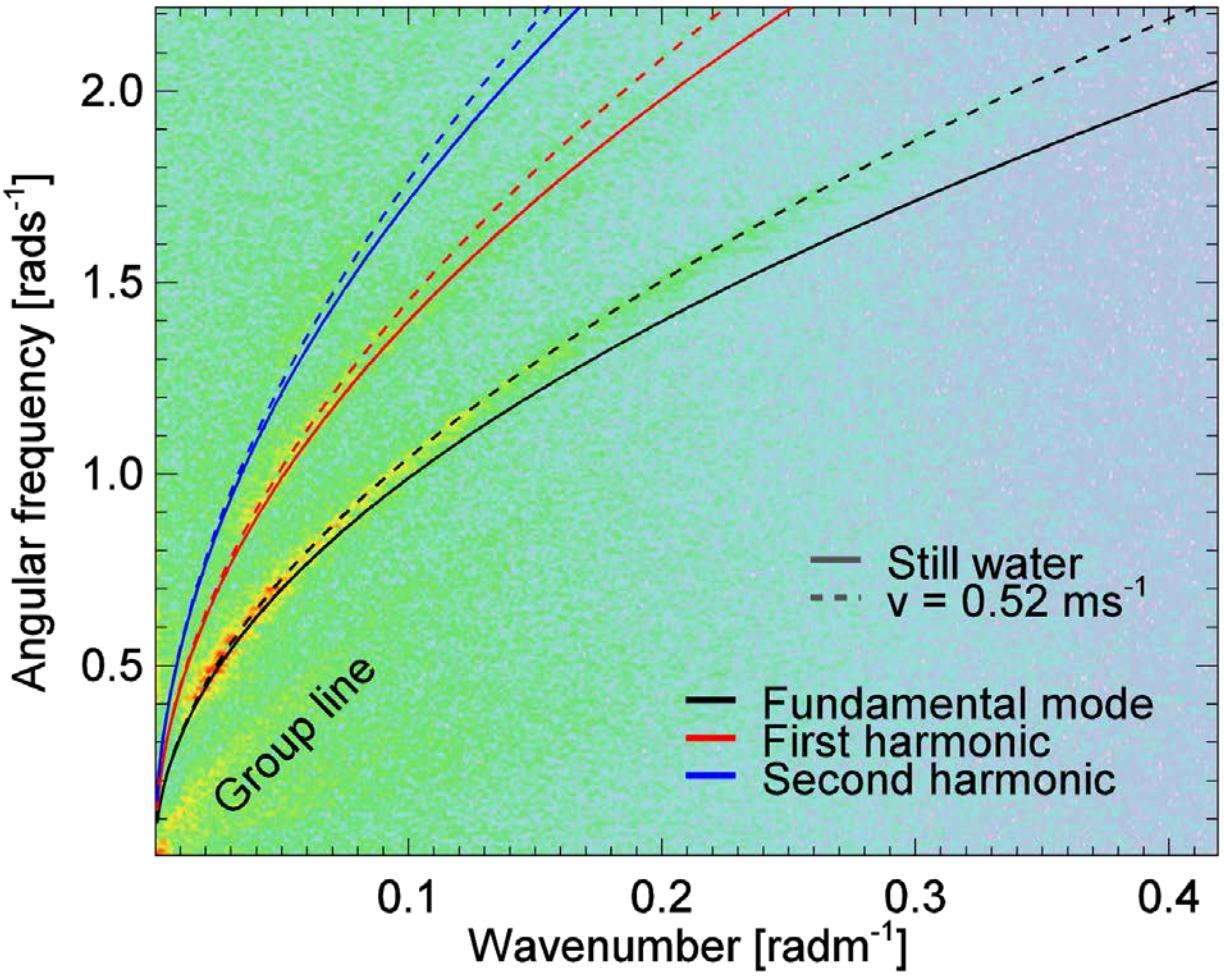

Figure 7 Reproduced from Figure 4 A. of Lund et al. [2015] (copyright American Meteorological Society) see the reference for full details. Cross-section through the 3D image spectrum in the peak wave direction. Wavenumber on the x-axis and angular frequency on the y-axis. "Still water" represents the open water, linear dispersion relation (without current) shown by a solid black line. The color code (blue to red) indicates the energy detected by MR. A speed of 0.52 ms^{-1} produces a good fit (black dashed line)

to the dispersion curve measured by the radar (energy significantly above the background noise level). Higher order harmonics are detectable in the MR spectrum.

Figure 6, reproduced from Lund et al. [2015], shows an example of this process. It represents a cross-section through one 3D image spectrum in the peak wave direction. Here we have wavenumber on the x-axis and angular frequency on the y-axis, we will refer to this as the dispersion plane. The colors in the background correspond to energy mapped to dispersion plane. The solid black line labeled "Still water" is the open water, linear dispersion relation (without current). Clearly, the energy detected by MR does not follow this curve. For a particular angular frequency, the wave numbers are lower (the wavelength is increased), from what one would expect from the linear dispersion relation. Using an iterative fitting process, the surface current which would result in such a Doppler shift matching the location of the energy is found. In this way, the surface current is always a byproduct of MR wave analysis. For the example above, a current of 0.52 ms^{-1} provided a Doppler shifted dispersion curve which was a good fit to the location of the energy on the dispersion plane.

In ice the dispersion relation will become the unknown, so an independent current measurement will be necessary. With **U** known, one can predict the expected Doppler term and hence deviation from the linear, open water dispersion relation so that any further deviation must be due to ice cover. Even in the absence of an independent current measurement, one might be able to make a rough guess at the dispersion relation if the currents calculated by MR are unreasonable.

Continuing the discussion on MR measurement, once the wave spectra are calibrated, MR may provide a spatio-temporal approach for calculating attenuation. The former technique requires open water and ice in a single image. If this is the case one could use different analysis boxes on a single image, marching into the ice, to determine attenuation. The main problem with this approach is that there is a known dependency of wave results on MR range and look direction [Lund et al., 2014]. A more robust approach would be to use the optimal field of view and over time go from open water to icy conditions.

Once dispersion and attenuation are known, and if[5] the other measurable properties of ice in visco-elastic models (ice thickness and elastic modulus) are known, then the visco-elastic dispersion relation can be inverted to give effective viscosity which is otherwise unmeasurable. This would be quite a feat.

[5]This is a huge *if* as there a many uncertainties related to the mechanical properties of ice (see Timco and Weeks [2010]).

2.1.4 Refraction and Shoaling

One of the important consequences of an altered dispersion relationship is the possible change in wave height. In direct analogy for refraction and shoaling in shallow water (or in currents), it can be shown that a change in group speed necessarily requires a change in direction and amplitude (this is Snell's law, most commonly encountered in the context of geometric optics). Furthermore, if the wavelength shortens, then the waves will turn, similar to a situation of waves approaching the shore: waves always turn to approach shore-normal (and vice versa if the wavelength elongates in ice). Let's imagine a situation where monochromatic waves of wavelength λ approach an ice field with properties which slowly vary over uniform contours. Wave crests approach the ice field some angle, θ, off-normal to the ice contour parallels and let ϕ be the corresponding angle between the wave crests and contour parallels. According to Snell's law, waves traveling in material 1 and 2 must obey the following relationship:

$$\frac{\sin\varphi_1}{\sin\varphi_2} = \frac{c_1}{c_2} = \frac{\lambda_1}{\lambda_2}$$

Where c is the group speed. The group speed in open, deep water (ow) follows from the linear dispersion relation:

$$\omega^2 = gk$$

$$c_g \equiv \frac{\partial\omega}{\partial k}$$

$$c_{g,ow} = \frac{1}{2}\sqrt{\frac{g}{k}}$$

As waves move into ice covered regions, Snell's law will determine the refraction angle:

$$\frac{\sin\varphi_{ice}}{\sin\varphi_{ow}} = \frac{\sin\theta_{ice}}{\sin\theta_{ow}} = \frac{c_{g,ice}}{c_{g,ow}} = \frac{k_{ow}}{k_{ice}} = \frac{L_{ice}}{L_{ow}}$$

The change in wave height is derived by conserving the mean energy per unit area, which can be determined from the spectrum by linear theory [Kinsman, 1965]:

$$E = 2\rho g\int_0^\infty S(f)df \ = \frac{1}{8}\rho g H_{m0}^2$$

The wave energy is simply the spectrum scaled by gravity and the density of water and the wave energy propagates at the group speed

$$P = EC_g$$

Assuming that the energy contained between two parallel rays is conserved along a section of crest width, s,

$$P_{ice}s_{ice} = P_{ow}s_{ow}$$

$$\frac{pg}{8}H_{m0,ice}^2 C_{g,ice}s_{ice} = \frac{pg}{8}H_{m0,ow}^2 C_{g,ow}s_{ow}$$

Solving for wave height in ice

$$H_{m0,ice} = H_{m0,ow}\left(\frac{C_{g,ow}}{C_{g,ice}}\right)^{\frac{1}{2}}\left(\frac{s_{ow}}{s_{ice}}\right)^{\frac{1}{2}} = H_{m0,ow}DK$$

Where D is the square root of ratio of the group velocities, which the appropriate $c_{g,ice}$ may be obtained from above.

$$D = \left(\frac{\frac{1}{2}\sqrt{\frac{g}{k_{ow}}}}{C_{g,ice}}\right)^{1/2}$$

K is the square root of the ratio of the crest lengths, from Snell's law above

$$K = \left(\frac{\cos\varphi_{ow}}{\cos\varphi_{ice}}\right)^{\frac{1}{2}}$$

The implication is this: if the group velocity slows in ice, then wave heights will increase (shoal) and if the group velocity increases in ice, then wave heights will decrease. In terms of the wave effects on ice, this will change the strain felt by the ice. Let say the group velocity decrease increasing the wave height: because of the increased wave height, ice-shoaled waves will put a greater (than expected from open water) strain on the ice leading to breaking events which might not otherwise occur. Over long distances, attenuation must be considered, and the net wave height will be a result of shoaling balanced against energy lost to dissipation or scattering. In addition, shortened wavelength and increased wave height increases steepness of the waves. The steepness may increase the likelihood that the waves will be unstable to modulational perturbations or breaking (see section 4.1), this has already been shown to be important for waves shoaling on an opposing current [Toffoli et al., 2015].

2.2 WAVE EFFECTS ON ICE

2.2.1 OVERVIEW

This document is admittedly biased towards ice effects on waves reflecting the first author's background in waves. There is rich body of research on ice mechanics, of which the effect of waves is only one of many possible influences. Here we attempt to summarize the more salient features of wave effects on ice.

Many wave effects on ice were previously mentioned. A short list includes the response to wave induced stress: recoverable strain (elasticity), elastic hysteresis, deformation (plasticity), creep, creep buckling (failure), elastic buckling (failure), creep crushing, continuous crushing, horizontal splitting, radial cracking, bending failure, non-simultaneous failures [Frannson, 2009]. Although this is a long list of specific terms, the connection between the wave field and these mechanics is often tenuous.

The most important, in terms of melting, is facture of the ice. Fracturing results in a geometrical or topological change which effectively increases the lateral surface area of the ice and accelerates the melting process through this increased exposure [Squire, 2007]. A much cited reference for lateral melting is Steele [1992], who used a simple ice-ocean model to show that, for conditions similar to those of summer time ice retreat, lateral melt was significant only for floes with diameters less than O(30 m). We should note here that the thermodynamics in this model are based on diffusion, that heat flux is proportional to surface area and that larger scale ocean dynamics, such as eddies, are not accounted for. Though the largest role played by the waves is increasing lateral surface area through breaking, it is also mentioned that waves in leads "can accelerate lateral melting near the surface" presumably due to mixing. Additionally, waves may over top and wash-over ice surfaces, which is currently being investigated as a new mechanism contributing to ice melting and reduced wave transmission [Skene et al., 2015; Toffoli et al., 2015].

2.2.2 Modeling Ice

Over an area of sea surface, the ice can be described by one or more of several properties: ice thickness distribution (ITD), floe size distribution (FSD), and ice concentration (IC). The ITD describes the percent surface area of ice attributable to a particular ice thickness, h. Similarly the FSD describes the percentage of surface area of ice attributable to ice of a diameter (some treatments consider caliper length), *l*. The concentration is the percent area covered by ice and typically acts to scale the influence of the ice.

CICE (Los Alamos Community Sea Ice Model) [Hunke et al., 2010] is a sophisticated, operationally run ice model based upon the continuity equation for ITD first described in Thorndike et al. [1975]. Waves have not played a role in CICE because their influence is limited to the MIZ which was traditionally a small part of the bulk ice field. However, the MIZs are increasingly accounting for higher percentages of the total ice coverage particularly in the summer months, and now account for >50% [Strong and Rigor, 2013]. How to get wave information into CICE, and what to do with it once it is there, is a topic of active research. By contrast, prognostic models based on continuity of FSD and joint floe size and thickness distribution (FSTD) are a very new development but wave physics arises naturally as a key player driving the their evolution [Zhang et al., 2015; Horvat and

Tziperman, 2015]. One path forward might be to use a FSD model, or breaking algorithm, as a mediator between a wave model and an ITD model.

We now dive a little deeper into the inner workings of an ice model by deriving a continuity equation using ice property, $\boldsymbol{p}$, which could be caliper length, diameter (for round floes), thickness, or some combination of these. The generalized distribution (which could be ITD, FSD, or FSTD) is then $d(\mathbf{p})$. Following Thorndike et al, [1979] $d(\boldsymbol{p})$ is area conserving, so that the integral over all ranges of ice property, $\boldsymbol{p}$, is unity.

$$\int_0^{\boldsymbol{p}_{max}} d(\boldsymbol{p}) d\boldsymbol{p} = 1$$

And the area, A, covered by ice within the property range $\boldsymbol{p}_1 \leq \boldsymbol{p} < \boldsymbol{p}_2$relative to the total area, R, is

$$\int_{\boldsymbol{p_1}}^{\boldsymbol{p_2}} d(\boldsymbol{p}) d\boldsymbol{p} = \frac{1}{R} A(\boldsymbol{p}_1, \boldsymbol{p_2})$$

The distribution evolves in space and time according to the prognostic continuity equation

$$\frac{\partial d(\boldsymbol{p})}{\partial t} = -\nabla \cdot (d\boldsymbol{u}) + \sum \mathcal{L}$$

This is the familiar fluid continuity equation, where the left-hand side is the change in time and the first term on the right-hand side is advection. In the second term on the right-hand side, $\mathcal{L}$ represents the different sources, sinks, and redistributors of the distribution of ice property. $\mathcal{L}$ consists of terms which parameterize the effects of mechanical interaction, thermodynamics, ridging/rafting and among others. Very recently, some work has been done to add a term to $\mathcal{L}$ which parameterizes the wave effects on FSD and FSTD which we will take up in the following sections.

For completeness we note that d(**p**), e.g. FSD, is not consistently defined in the literature. Here we have based the definition on area distribution in analogy with ITD. Also in use is number distribution, $N(\boldsymbol{p})$, and cumulative number distribution where

$$N(\boldsymbol{p}) = \frac{d(\boldsymbol{p})}{\pi \boldsymbol{p}^2}$$

2.2.3 Floe Size Distribution

Floe size distribution describes the number of floes of different sizes over an area. FSD is an important concept in the MIZ, as the pack ice in the central area of the Arctic is fairly uniform with large, indistinguishable floes with little or no open water. In the MIZ, as one goes from open water towards the pack ice, the FSD is characterized by large number of small floes with more open water and then a smaller number of larger floes with less open water.

The exceedance distribution (probability that a floe exceeds a particular size) is defined as

$$\mathbb{P}(l > l_*) = 1 - \int_0^{l_*} d(\boldsymbol{p}) d\boldsymbol{p} \quad for\ l > l_{min}$$

Here l is a parameter which describes the size of the floe and l_{min} is the minimum floe size considered. In reality, there is no limit to the minimum floe size, but practically, the minimum observable flow size depends on the resolution of the image. And the minimum floe size considered in primitive wave-ice interaction models is typically O(20 m) so that scattering based wave attenuation (which increases strength with the number of floes) doesn't become overly strong. This is obviously a problem for a coupled thermodynamic model because this leaves little overlap between minimum modeled floe size O(20 m) and the floe sizes most effected by lateral melt < O(30 m).

Observations of FSD [Rothrock and Thorndike, 1984; Toyota et al., 2006], done through analysis of aerial images, have shown exceedance distribution follows a power-law distribution with exponent, $-\gamma$. A power-law distribution implies scale invariance or fractal nature. Several studies have shown $\gamma \approx 2$ [Rothrock and Thorndike, 1984; Perovich and Jones, 2014]. Toyota et al. [2006] observed $\gamma = 1.87$ (also gives a range from 1 to 5) for floes greater than O(40 m) and $\gamma = 1.15$ for floes less than O(40 m). Apparently, wave induced breaking was the dominant mechanism for setting the exponent for smaller floes. Perovich and Jones [2014] observed an altogether departure from the power law behavior for smaller floes, hypothesized to be due to lateral melting. The consensus on a power law distribution is tenuous: as shown by Herman [2010], the scatter from one dataset to another is considerable and may be better fit by other distributions.

2.2.4 Primitive Wave-Ice Interaction Models

At the time of writing, there are only a handful of FSD models which handle coupled wave-ice interaction, so that we try to summarize the approach of each. There are two schools of thought, one which aims to develop a redistribution term for prognostic prediction of the FSD, and another which takes advantage of the parametric power-law description of FSD. Starting with the former, Thorndike et al. [1975] first used the general equation for non-local interaction of a property distribution for ITD due to ridging

$$\mathcal{L}_w = -Q(p)d(p) + \int_0^{\infty} \beta(p', p) Q(p') d(p') dp'$$

Zhang [2015] followed this approach for a redistribution function for FSD due to stochastic wave forcing. The ice property is caliper length. β is the redistributor of FSD and Q is the redistribution probability function. Under the constraint that $\int_0^{\infty} \beta(p', p) dp = 1$,

$$\beta(p', p) = \begin{cases} 1/(c_2 p_1 - c_1 p_1), & if \quad c_1 p_1 \le p_2 \le c_2 p_1 \\ 0, & if \quad l_2 < c_1 p_1 \ or \ p_2 > c_2 p_1 \end{cases}$$

c_1 and c_2 are redistribution coefficient constants defined by the minimum and maximum caliper size. The redistribution probability function is as follows:

$$Q(p) = \max\left[\left(1 - \int_l^{\infty} d(p')dp'/c_b\right), 0\right]$$

The open parameter here is c_b, the participation factor, which in general takes on a value $1 \geq c_b > 0$. This set up ensures that when floe sizes break, there is equal probability that any floe size bin smaller than the original floe bin size may gain from breaking (see the full reference Zhang [2015] for details). The result of breaking is then a FSD which obeys a power law distribution and puts the model in qualitative agreement with this feature of FSD observations.

Another approach is the wave focused studies of Williams et al. [2013a, b] which is based on the work of Dumont et al. [2011]. Here, a power law FSD is assumed, breaking then only adjusts the mean and maximum floe sizes. The minimum floe size is set to 20 m and the mean floe size is

$$\langle D^n \rangle = \frac{\gamma}{\gamma - n} D_{min}^n \tag{18}$$

Here γ is related to a breaking probability Π that a floe will break into ξ^2 pieces

$$\gamma = 2 + \log_{\xi} \Pi$$

Π is set to 0.9 and ξ to 2. This relationship and the values chosen are based on previous work by [Toyota et al., 2011]. This effectively gives $\gamma = 1.848$.

The model was motivated by the following scenario: imagine waves, as predicted by a 3G wave model, approaching the MIZ. Before entering the icy grid point, this model would take over and predict 1) the wave spectrum in icy waters and 2) the FSD throughout the MIZ subject to waves. Given an initial FSD and initial wave spectrum, the spectrum is marched into icy grid point where it is subject to attenuation due to the initial ice conditions. The ice-effected wave spectrum is used to calculate a significant strain on the ice based on plate theory:

$$\varepsilon = \frac{h}{2} \partial_x^2 \eta_{ice}$$

Here h is ice thickness and η_{ice} is the ice surface elevation. Since a wave spectrum is stochastic (random phase) and not deterministic, the strain exceedance probability function is developed based on the Rayleigh distribution:

$$\mathbb{P}_{\varepsilon} = \mathbb{P}(\varepsilon > \varepsilon_c) = exp(-\varepsilon_c^2 / 2m_0[\varepsilon])$$

Where

$$m_n[\varepsilon] = \int_0^\infty \omega^n S(\omega) \left[\frac{h}{2k_{ow}} k_{ice}^3 |\Im(\omega)|\right]^2 dw$$

$\Im(\omega)$ is a transmission coefficient and the critical strain is assumed, $\varepsilon_c = 3 \times 10^{-5}$. Given the length of time step and the zero-crossing wave-in-ice period, then the number zero-crossings is known and the exceedance probability may be evaluated. If critical strain level is exceeded, the floes break and then maximum floe size is set to half the dominant wavelength. Squire and Montiel [2015] offer small improvements by giving a nuanced definition for ice strength and including vertical variations of ice properties.

Horvat and Tziperman [2015] developed a prognostic equation for joint FSTD, similar in vein to Zhang [2015] but with explicit physics for the processes of freezing/melting, ridging/rafting, and breaking due to waves. The treatment of waves follows Williams et al. [2013a], but lacks some of the nuanced details. For example, instead of using a visco-elastic dispersion relation to derive wavelength, the open water dispersion relation is used. The model is quite sophisticated in other ways, and summarizing the rest of the model is outside the scope of this study but we encourage the interested reader to see the full paper.

To summarize, the following table describes the treatment of waves and ice published wave-ice interaction models.

Table 1 Summary of primitive wave-ice interaction and FSD models.

Study	Wave Treatment			Floe Treatment	
	Strain/Wave Height from Spectrum	Dispersion	Attenuation	Fracture	FSD calculation
Kohout and Meylan [2008]	Deterministic	Elastic (e.g. Fox and Squire [1994])	Scattering	Stress Criteria	N/A
Dumont et al. [2011]	Deterministic	Open Water	Scattering (Kohout and Meylan 2008)	Strain and Stress Criteria	Constrained by power law model (Eq. 18)
Williams et al. [2013a, b]	Probability Distribution Function	Visco-elastic (Robinson and Palmer [1990])	Viscous (Robinson and Palmer [1990]) and Scattering (Bennets and Squire, [2012]) (scattering dominant)	Stress Criteria	Constrained by power law model (Eq. 18)
Zhang [2015]	N/A	N/A	N/A	Parameterized	Constant distribution with parameterized min/max
Horvat and Tziperman [2015]	Stochastic	Open Water	Parameterized Scattering based on a fit to Kohout and Meylan [2008]	Stress Criteria	From wave information

Clearly there is much room for improvement and experimentation. On the side of wave physics, wave height is a stochastic process, so the probability of ice breaking is related to the wave height exceedance probability, in this case the Rayleigh distribution has been used extensively. The Rayleigh distribution was derived for linear, narrow banded wave spectrum. A simple improvement of the model would be to some other distribution (e.g. Tayfun and Fedele [2007]), but this is a fine tuning compared to the gross uncertainty in ice properties. For these models to significantly improve, we need much better observations of the mechanical properties of ice especially in concert with detailed wave measurements. We briefly address ice in the following section.

2.2.5 Ice Response

If the response of ice to stress is purely elastic (linear) a generalization of Hooke's law may be applied. Here the stress and strain are proportional with a coefficient known as the effective elastic modulus (Young's modulus). Under these linear conditions, the relationship between Lamé constants Young's modulus, the strain modulus, Poisson's ratio is derivable:

$$E = 2G(1 - v)$$

$$G = E/(2(1 - v))$$

$$v = \frac{E}{2G} - 1$$

Typically, the strain response of ice is not purely elastic either due to stress level effects such as yield or due cumulative stress effects such as creep strain [Timco and Weeks, 2010]. Under these conditions, the relationships above are not so clear, and the modulus relationships no longer describe the strictly linear portion of the stress strain relationship. Stress – strain relationship may still be described with effective modulus which include strain due to creep and inelasticity. The effective modulus of first year sea ice can be related to the brine content, v_b [Timco and Weeks, 2010]:

$$E = 10 - 0.351 v_b$$

Alternative formulas can be found in Squire and Montiel, [2015] and Appendix A. If the wave heights are high enough, the bending stress will exceed the fractural strength or the strain will exceed some critical strain. Unfortunately there are no definitive measurements of the mechanical properties of ice, and these mechanical properties are function of ice thickness, age, porosity, and salinity. Salinity may vary in the vertical cross section, giving a single slab mechanical properties with depend on the vertical dimension [Squire and Montiel, 2015]. For completeness, there is evidence that of ice fatigue due to repeat loading may be an important process [Langhorne et al., 1998].

2.2.6 ADVECTION

On larger scales, say time and space much larger than typical wave periods and lengths, the entire ice field may migrate as a result of a passing storm. Broström and Christensen [2008] (citing Perrie and Hu [1996]) report a migration up to 50 km per day. This amounts to surface velocity of O(0.5 ms^{-1}). This migration is driven by winds and currents, but wave induced Stokes drift and radiation stress must also play a direct role. On similar time scales, these same forces may cause the ice to converge and compress or diverge depending on if the forcing is directed into or out from the center of the pack ice, respectively. Of course, large wave effects are only possible with a sufficient fetch which necessarily implies the onto ice case. Small, fetch limited waves are theorized to play a role in ice band formation in the off-ice case [Wadhams, 2000].

2.3 FEEDBACK

Waves may change the nature of ice, and ice may then change the behavior of waves. This can occur on very fine scales, say fracturing a single ice floe which in turn modifies the scattering and attenuation the next wave encountered. On a larger scale, say during the passage of a single storm, waves propagate into the MIZ. Eventually the waves are attenuated by the ice, but the waves are also breaking up the ice which diminish one mechanism for attenuation. The waves continue to penetrate deep into the MIZ by fatiguing the ice along the way until (1) the ice is so strong that the waves may no longer pass or (2) the storm ends. This is a sort of equilibrium balance based on the strength of the ice and the power of the waves which enter into the MIZ. In this way the MIZ is always

in a state of non-equilibrium, changing based on the local environmental conditions [Wadhams, 2000].

This situation sets up the possibility of feedback loop in the system on a storm to storm scale. Continuing with the example of a storm passing through the MIZ from the open water. Waves generated during the storm will alter the MIZ. If through wave forcing there is significant melting/transport of ice would increases the fetch. An expanded fetch increases the potential of more energetic wave event occurring. If another, very similar storm follows in the same area, the waves will be bigger and the change in the ice that more dramatic, and the possibility of a feedback loop seems very serious [Asplin et al., 2012; Asplin et al., 2014; Thomson and Rogers, 2014; Collins et al., 2015]. Work is on-going to determine the importance of this feedback loop in the Arctic Ocean.

3 WAVE EVENT

3.1 SVALBARD 2010

The R/V Lance was in the vicinity of Hopen Island (Svalbard, NO) deep into the pack ice when it experienced a remarkable wave event. A full description of the wave event and measurements may be found in Collins et al. [2015]. The major findings of the study was an observation of binary behavior of wave – ice interaction for the peak waves. Meaning that the observations indicated that the peak waves were either not allowed (zero peak wave energy transmission) while the ice was unbroken, then quickly transitioned to total transmission of peak wave energy with fractured ice floes. Although low frequency waves were allowed, the high frequency (but low energy) waves were filtered according to the local floe size distribution. The change in local floe size distribution was a result of inhomogeneous (spatial gradient) and non-stationary (wave induced ice fracturing over time) ice conditions, though the relative contributions could not be determined.

Here we take up a few aspects of the wave event which were not fully explored in Collins et al. [2015]. The first is an estimation of detailed ice properties before the fracture event. This allows for an estimation of the flexural strength of the ice to make some inference about the necessary wave conditions. The second is the estimation of attenuation after the break up event.

3.1.1 SPECULATIVE FRACTURE INVESTIGATION (A. MARCHENKO)

Elastic ice is broken by waves when tensile stress at the ice surface or bottom reaches critical value, σ_{cr}, which is 2-3 times higher the flexural strength, σ_f [Marchenko et al., 2014]. Maximal stress at the surface of elastic ice sheet is calculated with the formula $\sigma = 0.5EhAk^2$, where E is the effective elastic modulus, h is the ice thickness, A is the wave amplitude, and k is the wave number. The effective elastic modulus is estimated with the formula of Vaudrey [1977], $E = 5.31\ \mathrm{GPa} - 0.436\sqrt{v_b}\ \mathrm{GPa}$, where v_b is the liquid brine content of the ice calculated with Frankenstein and Garner [1967] formula v_b = S(48.185/|T| + 0.532). Mean values of sea ice temperature, T, salinity, S, and flexural strength measured in the Van Mijen Fjord (Spitsbergen) in 1-3 May 2010 were T = -1.93°C, S = 3.9 ppt, and σ_f =142.5 kPa. Therefore liquid brine content was v_b = 100 ppt, and E = 0.95 GPa. Critical tensile stress at the ice surface is estimated as 285 < σ_{cr} < 427.5 kPa. The observed wave length was 125.6 m corresponding to the wave number k = 0.05 m^{-1}. Assuming ice thickness h = 0.6 m the critical wave amplitude is estimated as 0.37 < A < 0.56 m. Waves with higher amplitudes should fracture sea ice immediately. Langhorne et al. [1998] investigated the reduction of flexural strength on 60% due to the fatigue failure effect. In our case it means a reduction of critical wave amplitude to the range 0.22 < A < 0.34 m. Waves with higher amplitudes will fracture sea ice by low frequency fatigue during 10 to 100 cycles of the wave action. Wave period in our case is 12.5 s. Therefore representative time of the fatigue fracture is varying from 125 s to 20 min.

3.1.2 Post Fracture Attenuation Rates

Attenuation rates are calculated as a function of period, T, using the following relationship:

$$\alpha_n(T) = \frac{\ln(S_{n+1}/S_n)}{D_n}$$

Here $S_{n+1}(f)$ is the attenuated wave spectra of original form $S_n(f)$. S(f) is either measured of provided by model application. D_n is the effective distance through ice which the spectra has propagated. A major assumption is stationarity of the wave and ice fields during the analysis period (here 1 hour). Below we explore different methods of determining D_n and use both measured and modeled $S(f)$.

3.1.2.1 METHOD 1: ALONG THE SHIP TRACK

Starting with the four spectra measured below. S_1, S_2, S_3, and S_4 correspond to spectra measured from R/V Lance at 02 23:24, 03 00:30, 03 02:30, and 03 03:30, respectively.

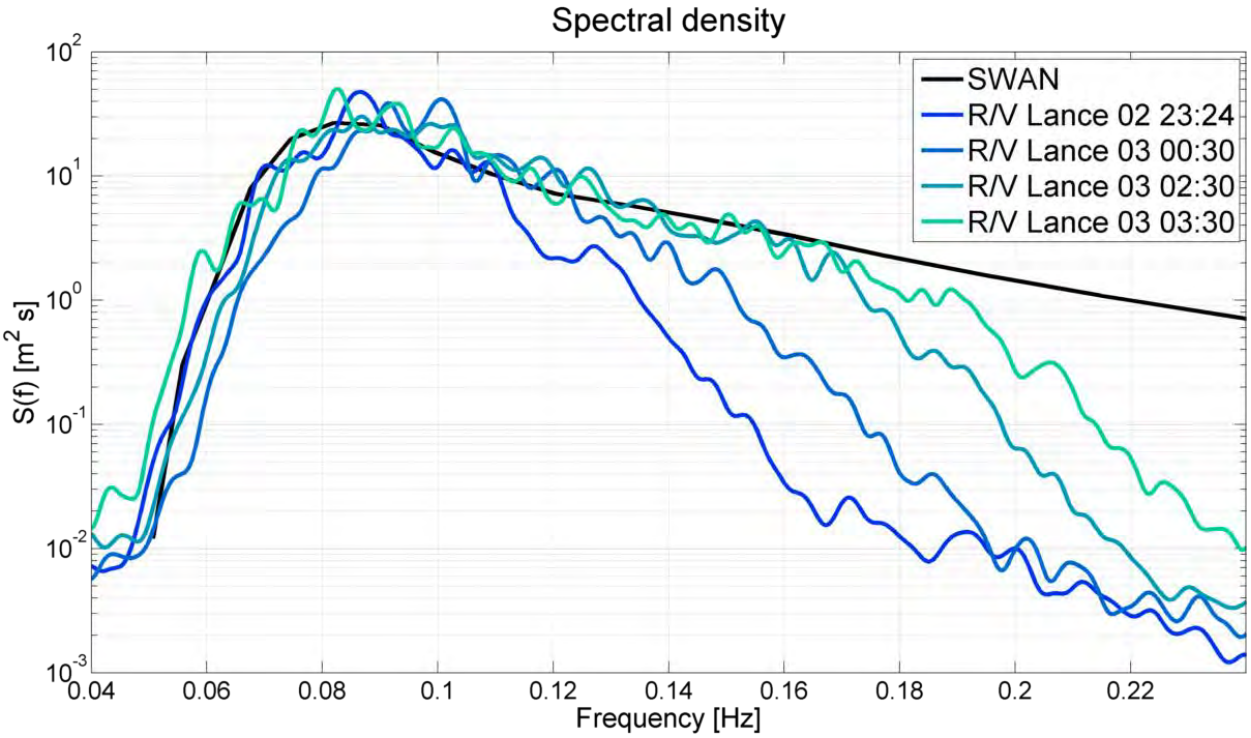

Figure 8 Spectral evolution over the course of five hours. The black line is the SWAN "no ice" reference. The colored spectra are calculated from the sea surface elevation signal from R/V Lance and move forward in time from dark blue to green.

Where in the attenuation equation, D_n is the distance between the mean position during measurement of S_n and the mean position during measurement of S_{n+1}. This assumes that the waves are traveling in the opposite direction of the vessel. There is not a convincing argument justify this assumption, however it should result in at least the right order of

magnitude. For our three cases D_1 = 10.1 km, D_2 = 18.7 km, D_3 = 9.9 km. Leading to the following attenuation rates as a function of wave period (T).

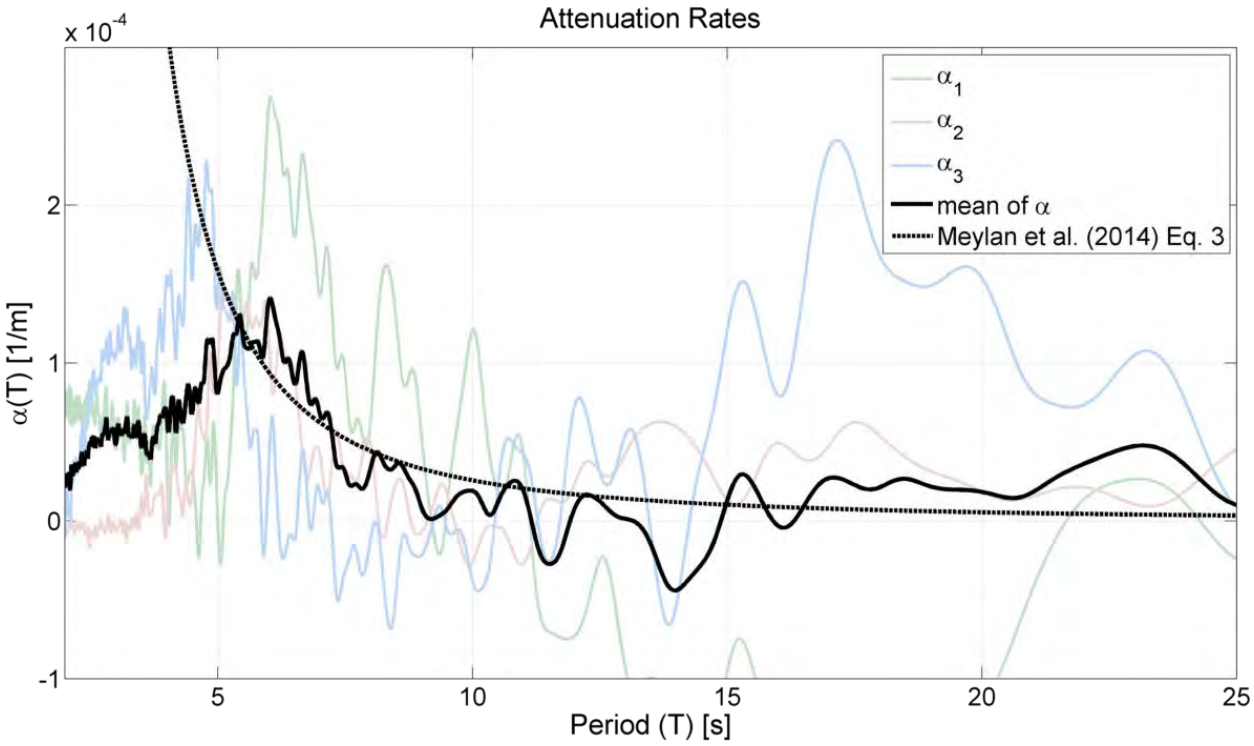

Figure 9 The spectral attenuation rates as a function of wave period. The light colored lines are the individual calculations and the black line is their mean. The dotted line is the empirical model from Meylan et al. [2014].

Shown is the three attenuation rates calculated from the spectra above in light colors and their mean shown with the solid black line. The dotted black line is Eq. 3 from Meylan et al. [2014]:

$$\alpha_M(T) = \frac{a}{T^2} + \frac{b}{T^4}$$

Where coefficients a (2.12×10^{-3}) and b (4.59×10^{-2}) were fit from their measurements. The agreement between the mean measured α and α_M is suspiciously good.

3.1.2.2 METHOD 2: ICE CONTOURS FROM PIPS

Let us consider an alternative definition of D_n from the relative distance traveled into the ice. This is done by comparing the length of rays parallel to the mean direction at the peak of the spectrum as output by WWIII. This assumes that the wave direction is the same at all frequencies and does not change with entering the ice. We track the change in distance to the 75 % ice concentration contour given by an ice model called PIPS as shown in the figure below. The assumption here is that the 75 % ice contour, given in the figure below, from before the storm is characteristic of the ice concentration during the storm maintains shape over the course of these 4-5 hours.

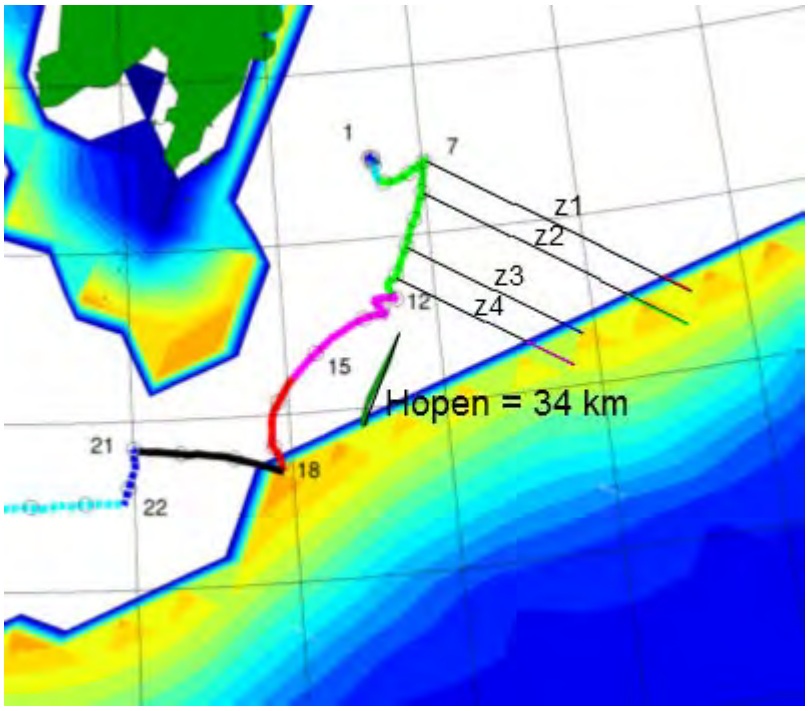

Figure 10 Map showing southern tip of Svalbard, Norway including Hopen Island (all marked in green). The ice concentration is a product of the PIPS model and given by the colored contours with the white indicating the 75 % concentration contour. The ship track is marked in color and the distances to the 75 % contour are given parallel to the dominant wave direction as given by WW3 and represented by z_1, z_2, z_3, and z_4.

The length of black line segment which spans Hopen Island is approximately 34 km giving a conversion rate from image pixels to km. This segment is rotated to be parallel to the white arrow showing wave direction while retaining the length. This is then copied until it crosses the 75 % contour and the remainder is measured in pixels and converted to km. The absolute distances for the four segments are z_1 = 89.9 km, z_1 = 77.9 km, z_1 = 59.4 km, and z_4 = 29.3 km. The relative distances for our three cases becomes D_1 = 12.0 km, D_2 = 18.4 km, D_3 = 10.3 km (compare to path defined D_1 = 10.1 km, D_2 = 18.7 km, D_3 = 9.9 km). This doesn't significantly alter the attenuation rate, but the mean attenuation rate fits the empirical model slightly better.

3.1.2.3 METHOD 3: ICE CONTOURS AND SWAN

Considering yet another way to estimate attenuation rates is to use the spectra from SWAN (black spectra in Figure 8). This will give us four attenuation rates (1 per measured spectra) vs. the three from measured spectra only. This assumption is the SWAN provides an estimate of spectra from the ice free open waters. The problem is again to determine an appropriate $D_{n.}$, but the nuance here is that relative distance is no longer sufficient, we need to estimate absolute distance the waves have traveled into the ice. We start by using the values of z_n as defined above as first guess.

As simple way to vary the distance D_n is to scale the attenuation rate. So that multiplying the attenuation rate by 2 is effectively cutting the distance, D_n, in half. Likewise multiplying by 4 is quartering the distance.

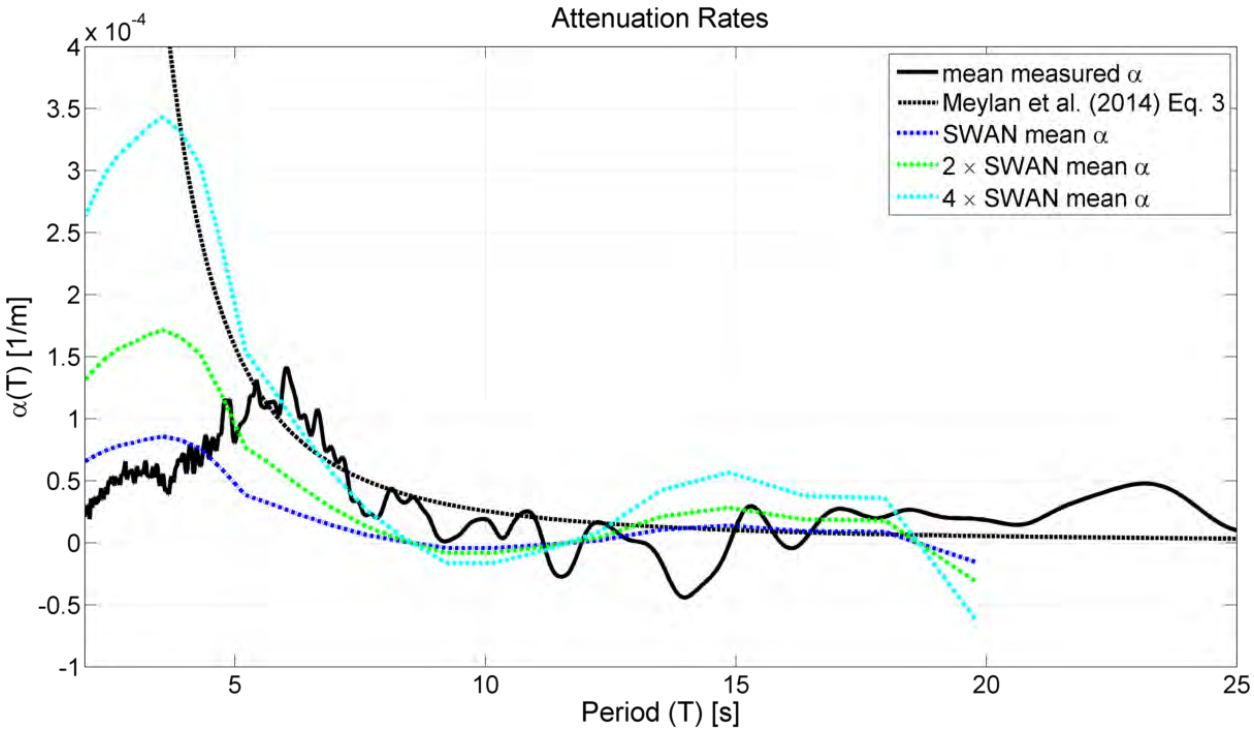

Figure 11 same as Figure 9 with the addition of colored dashed lines representing the mean attenuation rates using SWAN. The colors blue, green, and cyan represent scaling of 1, 2, and 4, respectively.

Figure 11 shows the mean of the 4 attenuation rate estimates using SWAN spectra. The initial guess at the D_n give attenuation rates which fell under the empirical model from 5 – 15 s (expected effective range) but matched from 15 – 20 s (outside the expected effective range). By quartering the distance, we get attenuation rates that better match the empirical model from 4 – 8 s but slightly underestimate the model from 8 – 12 s and slightly overestimate thereafter. This may indicate: 1) a deficiency in the attenuation model, 2) D_n was actually much shorter than indicated by PIPS (possible mid-way through the storm), 3) deficiency in SWAN or measured spectra, and 4) all of the above.

For sake of completeness, the ice edge could have been defined at any contour (i.e. 50 %, 20 %) or by scaling it, e.g. integrating for distance X but instead of using the entire distance use dx*C where C is concentration as a fraction. All of these would have increased the distance D_n and lessened the agreement in the range of periods where attenuation is expected.

Calculating distance from the ice edge is one part of the problem, but the other part is ice is changing in time, both due to bulk migration of ice and the advection of the ship

through the ice, so it's possible that we would get a similar migration (in frequency space) of the low-pass filter even with the ship staying in one place.

4 SPECULATIONS AND CONCLUSIONS

4.1 LARGE WAVE EVENTS

Recently, a hypothesis has been put forward that large waves, in particular large swell, behave quite differently in ice than lower height swell and even large wind sea. This is still very much new territory, but we may make a few speculations here in the hopes that future studies may be able to confirm or deny.

Several studies report ice breakup due to wave forcing deep into the pack ice. The account of chief scientist of the R/V Polarstern, E. Augstein, was reported in Liu and Mollo-Christensen [1988] and further expanded on in Broström and Christensen [2008]. Approximately 560 km from the ice edge, waves of 1 m height and 18 s period broke up ice and caused significant rafting. The wavelength before the ice broke was reported to be smaller than the wavelength in broken ice which motivated his formulation of the dispersion relation with compressive stress.

Kohout et al. [2014] claim that, for particular wave periods, wave heights greater than 3 m are linearly attenuated by ice vs the typical exponential attenuation which they found still described waves of heights less than 3 m. In this and more recent studies [Kohout et al., 2015; Li et al., 2015] they argued that the difference in attenuation is due to non-linear wave-wave interaction. That effectively, the lower frequencies continue to receive energy from higher frequencies as a result of the energy flux dictated by S_{nl}.

In our estimation, S_{nl} acts over long time and space scales, where, presumably the nature of the ice will be changing significantly, so in practice it is very difficult to isolate the influence of S_{nl}. Furthermore, S_{nl} is very weak for typical ocean swell (e.g. Young and Van Vledder [1993]) meaning for the classic case of swell interning ice, S_{nl} is likely unimportant. There is, however, an open question to how a change in dispersion might affect S_{nl} (e.g. Polnikov and Lavrenov [2007]).

In contrast to the longer scale non-linearity associated with resonant wave-wave interaction, S_{nl}, Collins et al. [2015] brings attention to shorter scale, off-resonant wave-wave interaction (i.e. modulation instability) first discussed in the context of ice by Liu et al. [1988]. In terms of attenuation, after pack-ice was broken into floes, there was little if any attenuation for large, low frequency waves (which is also in agreement with results of Doble and Bidlot [2013]). They used MI to explain how waves are able to march into pack ice to begin with, but not to explain the different regimes of wave-ice interaction (i.e. differences in wave attenuation). Low frequency waves of the size measured in Collins et al. [2015] have never before been measured in the Arctic (see Appendix B). The regimes of

wave ice interaction were seemingly controlled by the ice, i.e. whether the ice was solid or fractured. It is possible that the analysis of Kohout et al. [2014] rolls the two together and gets significantly different attenuation for large waves because the ice is fractured (fracturing perhaps requiring such large waves) effectively convoluting the two issues (ice state and sea state). Unfortunately, there is not enough experimental information necessary to determine if there are fundamentally different interaction regimes for large waves then for small waves, but certainly the above studies suggest a real need for more comprehensive observations. There are several issues which need attention: (1) accurate measurement of the attenuation/dispersion during and after the ice breakup, (2) modification of regular wave growth and decay in ice, and (3) better observations of the ice break up process.

4.2 WAVES AS A SOURCE OF HEAT?

It has long been known that energy lost to waves from breaking goes primarily to turbulence through the energy cascade and ultimately to heat via viscosity. This heat generation was recently estimated in the context of surf zones by Sinnett and Feddersen [2014]. Two factors make it plausible that this mechanism contributes significantly to the water temperature in the surf zone at some beaches. First, in the surf zone, dissipation occurs over small horizontal distances, so dissipation per unit area is much larger than in the open ocean, where active whitecaps cover only a very small fraction of the surface at any instant. Second, the water is shallow, so the heat cannot be mixed into lower, cooler water. Neither of these two factors necessarily applies to the MIZ, where dissipation occurs over larger horizontal distances, and water is deeper. However, it offers an intriguing possibility, that there is this additional mechanism by which waves contribute to accelerated ice melt or decelerated ice freezing. In any case, it should not be totally dismissed and it may be worthwhile in the future to estimate this effect.

Perhaps more interesting is the possibility that the repeated bending of ice sheets and large ice floes by wave action causes fatigue (i.e. hysteresis or internal friction) in the ice, which results in heat. What effect would this have on the strength of the ice and its capacity to support further strain? However, one could easily make the counter-argument that the thermal and mechanical effects of the bending on the ice would be so difficult to estimate separately in practice, that they would logically be lumped together in any predictive model.

4.3 FINAL THOUGHTS

In this document we have summarized the nature of ice effects on waves and waves on ice. From a theoretical point of view, the ice effects on waves is much more developed. We explored several formulations of the in ice dispersion relation in some detail. We used an example visco-elastic model to better understand the change in dispersion and the expected attenuation once waves inter icy waters. The wave effects on ice are intuitive: the may break ice up and move it around, but models of these process are very primitive.

On the measurements side, attenuation is well documented but there are large differences between studies due in part to the variable nature of ice. The nature of ice, its physical and mechanical properties, are a stumbling block that needs to be overcome in future studies. Measurements of dispersion are lacking, but the potential for making such measurements with marine radar is seemingly good. Primitive, two-way wave and ice floe size distribution models are immerging which are hopefully the vanguards of future operational systems. Before this can happen, two broad issues need to be addressed: 1) a consistent definition of FSD needs to be determined and used in the literature and 2) continued observations of FSD which might be used to compare to the models. In particular a description of FSD is needed which either definitively supports or challenges and supersedes the current power law based models.

The wave-ice interaction problem is difficult, in some cases intractable, because of the disparate scales involved and the varied nature of ice in the field. With the ONR Sea State field experiment underway, there is the looming prospect of high quality field data and new theoretical tools which we hope will usher in new breakthroughs in wave-ice physics. Here we must face that no matter how comprehensive a measurement campaign, developing a model which can predict two-way coupled behavior of waves and ice over all the various scales is a daunting task. Nonetheless, we have never been so well equipped to undertake such challenges and the prospects for progress are favorable.

ACKNOLEDGMENTS

C.O.C. is grateful to the ASEE and NRL for fellowship funding at NRL SSC. W.E.R. acknowledges the support of ONR grant N0001413WX20825. Vernon Squire and Johannes Mosig provided useful comments, corrections, and guidance for section 2.1. Chris Horvat provided insightful comments which greatly enhanced section 2.2. Björn Lund greatly improved the text in section 2.1.3.4. Many thanks to the captain and crew of the R/V Lance.

APPEDDIX A: BENDING AND DISPERSION OF VISCOELASTIC WAVES (MARCHENKO)

A.1 BENDING MOMENT IN ICE PLATE WITH ELASTIC AND CREEP RHEOLOGICAL PROPERTIES

Two dimensional bending deformations of floating solid ice caused by wave induced water pressure below the ice are described by equations of static equilibrium

$$\frac{\partial \sigma_{xx}}{\partial x}+\frac{\partial \sigma_{xz}}{\partial z}=0\,,\ \frac{\partial \sigma_{xz}}{\partial x}+\frac{\partial \sigma_{zz}}{\partial z}=\rho_i g\,, \tag{1a}$$

where x and z are the horizontal and vertical coordinates, $\sigma_{ij}\ \ (i,j=x,z)$ are the ice stresses, and ρ_i is the ice density. Ice inertia is ignored in comparison with inertia of the water involved in the wave motion. It is valid when wave lengths and water depth are much greater the ice thickness.

Linearized boundary conditions have the following form

$$\sigma_{zz}=-p_a\,,\ \sigma_{xz}=0\,,\ z=h/2\,;\ \sigma_{zz}=p_w\,,\ \sigma_{xz}=0\,,\ z=-h/2\,, \tag{2a}$$

where p_a is the atmosphere pressure, and p_w is the water pressure below the ice.

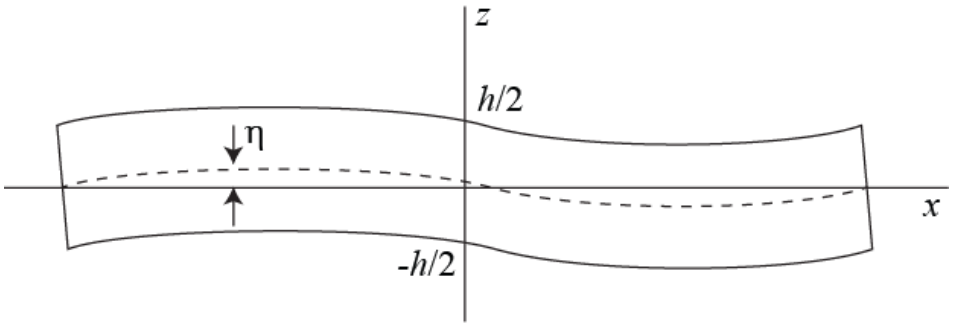

Figure A-1. Ice plate floating on the water surface.

Multiplying the first equation (1) on z and integrating it over z from $z=-h/2$ to $z=h/2$ we find

$$\frac{\partial M_{xx}}{\partial x}-N_x=0\,,\ M_{xx}=\int_{-h/2}^{h/2} z\sigma_{xx}dz\,,\ N_x=\int_{-h/2}^{h/2}\sigma_{xz}dz\,. \tag{3a}$$

Integration of the second equation (1) over z lead to the equation

$$\frac{\partial N_x}{\partial x}=\rho_i g h-\Delta p\,,\ \Delta p=p_w-p_a\,. \tag{4a}$$

Combination of equations (3) and (4) gives

$$\frac{\partial^2 M_{xx}}{\partial x^2} = p_a - p_w . \tag{5a}$$

Link between bending moment M_{xx} and water surface elevation η is established by the use of rheological equations. We assume plane strain state in the ice with respect to the axis y perpendicular to the plane (x, z). We assume creep rheology of ice for the stress deviator and elastic rheology for the pressure

$$\dot{\varepsilon}_{el} + \dot{\varepsilon}_{cr} = \frac{\partial(\varepsilon_{xx} - \varepsilon_{zz})}{\partial t},\ \sigma_{xx} + \sigma_{zz} = 2(\lambda + \mu)(\varepsilon_{xx} + \varepsilon_{zz}), \tag{6a}$$

where λ and μ are effective elastic constant, and $\dot{\varepsilon}_{el}$ and $\dot{\varepsilon}_{cr}$ are elastic and creep strain rates. Elastic strain rate is determined by the formula

$$\dot{\varepsilon}_{el} = \frac{1}{2\mu}\frac{\partial(\sigma_{xx} - \sigma_{zz})}{\partial t}. \tag{7a}$$

Elastic constant are expressed by the formulas

$$\mu = \frac{E}{2(1+\nu)},\ \lambda = \frac{E\nu}{2(1+\nu)(1-2\nu)}, \tag{8a}$$

where E is the effective elastic modulus, and $\nu \approx 0.33$ is the Poisson's ratio of ice. The elastic modulus is calculated with the formula (Vaundray, 1977)

$$E = 5.31 - 0.436\sqrt{\nu_b}. \tag{9a}$$

where ν_b is calculated in ppt. Liquid brine content ν_b is calculated as follows (Frankenstein and Garner, 1967)

$$\nu_b = S_{si}\left(\frac{48.185}{|T_{si}|} + 0.532\right),\ -22.9^{\circ}\mathrm{C} < T < -0.5^{\circ}\mathrm{C}, \tag{10a}$$

where T_{si} and S_{si} are the temperature and salinity of sea ice averaged over ice thickness.

Creep strain rate is expressed by the formula (Durham et al, 1997)

$$\dot{\varepsilon}_{cr} = K\,|\,\sigma_{xx} - \sigma_{zz}\,|^3\,(\sigma_{xx} - \sigma_{zz}), \tag{11a}$$

where creep constant K could expressed in terms of representative strain rate ($\dot{\varepsilon}_0$) and stress (σ_0) in creep tests: $K = \dot{\varepsilon}_0\sigma_0^{-4}$. Assuming that $\dot{\varepsilon}_0 = 10^{-6}\,\mathrm{s}^{-1}$ and $\sigma_0 = 1\,\mathrm{MPa}$ (Cole et al, 1998) we estimate $K = 10^{-6}\,\mathrm{s}^{-1}\mathrm{MPa}^{-4}$.

It is assumed that bending deformations of floating ice are caused by surface waves with period about 10 s and wavelength 125 m. Maximal elastic stress caused by wave induced bending deformations of floating elastic ice plate is estimated by the formula

$$\sigma_{el} = \frac{Ehak^2}{2(1-\nu^2)}, \tag{12a}$$

where a and k are wave amplitude and wave number. Assuming $h = 0.5\,\mathrm{m}$, $E = 2\,\mathrm{GPa}$, $a = 0.5\,\mathrm{m}$ and $k = 0.05\,\mathrm{m}^{-1}$ we find $\sigma_{el} = 1.25\,\mathrm{MPa}$.

For the comparison of the terms in the left side of the first equation (6) we assume that $\sigma_{xx} - \sigma_{zz} = \sigma_{el}$. The ratio of elastic strain rate to creep strain rate is equal

$$\frac{\dot{\varepsilon}_{el}}{\dot{\varepsilon}_{cr}} = \frac{\omega}{EK\sigma_{el}^3}, \tag{13a}$$

where $\omega = 0.6\,\mathrm{s}^{-1}$ is the wave frequency. Numerical estimates show that $\dot{\varepsilon}_{el}\dot{\varepsilon}_{cr}^{-1} \approx 1.5 \cdot 10^2$, i.e. creep strain rates are much smaller than elastic strain rates.

From equations (3) and (5) follows that $M_{xx} \approx \sigma_{xx} h^2$ and $M_{xx} k^2 \approx p_w$ when the ice is deformed by a wave with wavelength k. Therefore $p_w \approx \sigma_{xx} h^2 k^2$ and $p_w << \sigma_{xx}$ when $h^2 k^2 << 1$. Further this fact is used for the construction of solution of rheological equations (6).

Solution of equations (6) is constructed by the method of successive approximations with the first term describing pure elastic solution

$$\sigma_{0,xx} - \sigma_{0,zz} = 2\mu(\varepsilon_{xx} - \varepsilon_{zz}), \qquad \sigma_{0,xx} + \sigma_{0,zz} = 2(\lambda + \mu)(\varepsilon_{xx} + \varepsilon_{zz}). \tag{14a}$$

Assuming that $\sigma_{0,xx} >> \sigma_{0,zz}$ we find $\sigma_{0,xx} = E(1-\nu^2)^{-1}\varepsilon_{xx}$. Taking into account the Kirchoff's hypothesis (Timoshenko and Woinovsky-Krieger, 1959) the final form of the first order approximation is

$$\sigma_{0,xx} = -\frac{zE}{1-\nu^2}\frac{\partial^2 \eta}{\partial x^2}, \tag{15a}$$

where η is the deflection of the mid-surface from the horizontal plane (Fig. 1).

In the next order of the approximation we assume that $\sigma_{xx} = \sigma_{0,xx} + \sigma_{1,xx}$, where stress $\sigma_{1,xx}$ accounts the influence of creep effect and calculated from the equation

$$\frac{1}{2\mu}\frac{\partial \sigma_{1,xx}}{\partial t} + K\left|\sigma_{0,xx}\right|^3 \sigma_{0,xx} = 0. \tag{16a}$$

From equations (15) and (16) follows that bending moment is determined by the equation

$$\frac{\partial M_{xx}}{\partial t} = -D_{el}\frac{\partial}{\partial t}\frac{\partial^2 \eta}{\partial x^2} + D_{cr}\left|\frac{\partial^2 \eta}{\partial x^2}\right|^3 \frac{\partial^2 \eta}{\partial x^2}, \tag{17a}$$

$$D_{el} = \frac{Eh^3}{12(1-\nu^2)},\ D_{cr} = \frac{K\mu h^6}{96}\left(\frac{E}{1-\nu^2}\right)^4.$$

A.2 DISPERSION EQUATION FOR THE WAVES PROPAGATING IN IDEAL FLUID BENEATH AN ICE PLATE WITH ELASTIC AND CREEP PROPERTIES

Linearized kinematic and dynamic boundary conditions at the surface of ideal fluid covered by the ice plate are written as follows

$$\frac{\partial \eta}{\partial t} = \frac{\partial \varphi}{\partial z},\ \frac{\partial \varphi}{\partial t} + g\eta - \frac{1}{\rho}\frac{\partial^2 M_{xx}}{\partial x^2} = 0,\ z = 0, \tag{18a}$$

where φ is the velocity potential in the fluid, η is the water surface elevation, and ρ is the ice density. Bending moment M_{xx} is expressed by η using equation (17). Boundary conditions (18) are reduced to the boundary conditions at the surface of ideal fluid covered by elastic plate when $D_{cr} = 0$.

Substituting in equations (17) standard expressions for the water velocity potential and water surface elevation describing surface waves in the fluid with depth H

$$\varphi = \varphi_0 e^{i(kx+\omega t)}\frac{\cosh[k(z+H)]}{\cosh[kH]} + C.C., \qquad \eta = Ae^{i(kx+\omega t)} + C.C.,$$

(19a)

we find the dispersion equation

$$\omega^2 = \omega_{fgw}^2 + i|A|^4\Delta,\ \Delta = D_{cr}k^8/\rho, \tag{20a}$$

$$\omega_{fgw}^2 = k\tanh[kH]\left(g + D_{el}k^4/\rho\right).$$

APPENDEX B: WAVE HEIGHTS MEASURED IN ARTIC ICE

Here, to support our claim to have measured the largest waves in ice in the Arctic region, we have attempted to make an exhaustive review of the literature. An earlier version of this appendix was published as supplemental material for [Collins et al., 2015].

Studies report wave height using a variety of metrics. In studies where the individual maximum wave height, H_{max}, or the root-mean-square wave height, H_{rms}, was reported, we use a simple formula to convert to the spectral significant wave height, H_{m0}. Considering typical wave periods and analysis times, the following relationships derived from a Rayleigh distribution are roughly applicable (e.g. Holthuijsen [2007]).

$$H_{m0} = 1.4H_{rms} = 0.5H_{max}$$

When only the energy (or variance) density is reported for a particular spectral band, an attempt is made to estimate a JONSWAP spectrum [Hasselmann et al., 1973] based on the energy level at the peak frequency. This is done in a conservative manner such that the estimation of H_{m0} is an upper limit (or perhaps slightly overestimated).

We tried to be thorough, but invariably there will be studies which were passed over or could not be verified. One that fits into the latter category is work by P. Wadhams, in which the measurement of wave heights was made by an inverted echo sounding from a submarine [Wadhams, 1972; Wadhams, 1978]. Though these citations are indexed (e.g. google scholar, web of science) actual records (proceedings in the first case, an article in the second) could not be located.

As far as the Arctic region (see Table S1) is concerned, our study is by far highest and is similar to wave heights observed in the ice free measurements of Thomson and Rogers [2014] in the Beaufort Sea. As it may be of interest, we have also tabulated the cases of waves measured in ice in the Antarctic as well (see Table S2).

Table 2 Summary of the published accounts of waves measured in ice in the Arctic region.

PUBLICATION	STUDY YEAR	LOCATION	METHOD	WAVE HEIGHT (H_{M0})
[Fakidov, 1934]	1933-1934	Arctic Ocean	Visual	<< 1 m
[Crary et al., 1952]	1951	Arctic Ocean	Gravity Meter	5×10^{-4} m
[Hunkins, 1962]	1957-1958	Beaufort Sea	Gravity Meter[6]	<< 1 m
[Wadhams, 1975]	1972	Canadian North Atlantic[7]	Airborne Laser	~2 m
[Squire and Moore, 1980]	1979	Bering Sea	floe-borne accelerometers	~1.5 m
[Wadhams et al., 1986; Wadhams et al., 1988]	1978, 1979, & 1983	Bering Sea and Greenland Sea	Buoys	~1 m
[Liu et al., 1991]	1989	Labrador Sea	Buoy	~2.6 m
[McKenna and Crocker, 1992]	1989	Labrador Sea	floe-borne accelerometers	~0.5 m
[Rottier, 1992]	1989	Barents Sea and Fram Straight	Buoy	~0.75 m
[S. Frankenstein et al., 2001][8]	1990	Barents Sea	floe-borne accelerometers	?
[Marko, 2003]	1998	Sea of Okhotsk[9]	ADCP	~1.5 m
[Asplin et al., 2012]	2009	Beaufort Sea	3-D ship-borne recorder	~0.75 m
This Study	**2010**	**Barents Sea**	**Ship GPS**	**4-5 m**

[6]There are other studies which analyze the observations of gravity meters, seismometers, or tiltmeters deep in the ice field (see the references in Wadhams [1975]), all of which record small (O(1×10^{-4} m)) vibrations of the ice.
[7]Not within the Arctic region.
[8]An event very similar to the one reported in out manuscript was described, but measurements were not made during it.
[9]Not within the Arctic region.

Table 3 Summary of the published accounts of waves measured in ice in the Antarctic region.

PUBLICATION	STUDY YEAR	LOCATION	METHOD	WAVE HEIGHT (H_{M0})
[Robin, 1963]	1959-1960	Wendell Sea	Ship-borne Recorder	~0.5 m
[Liu and Mollo-Christensen, 1988]	1986	Wendell Sea	Visual	~1 m
[Crocker and Wadhams, 1988]	1986	Ross Sea	Wire Strainmeter	<< 1 m[10]
[Fox and Haskell, 2001]	1998	Ross Sea	Floe-borne recorder	?[11]
[Hayes et al., 2007]	2003	Bellinghausen Sea	ADCP on an AUV	~ 3 m
[Doble and Bidlot, 2013]	2000	Wendell Sea	Buoy	~10 m
[Meylan et al., 2014; Kohout et al., 2014]	2012	Antarctic Ocean	Floe-borne recorder	~6 m

[10]Measured strain (not amplitude), a conversion depended on Young's modulus (not measured).

[11]Measurements shown only in terms of acceleration and acceleration spectra.

REFERENCES

Ardhuin, F., E. Rogers, A. Babanin, J. Filipot, R. Magne, A. Roland, A. Van Der Westhuysen, P. Queffeulou, J. Lefevre, and L. Aouf (2009), Semi-empirical dissipation source functions for ocean waves: Part I, definition, calibration and validation. Journal of Physical Oceanography, 40(9), 1917-1941.

Asplin, M. G., R. Galley, D. G. Barber, and S. Prinsenberg (2012), Fracture of summer perennial sea ice by ocean swell as a result of Arctic storms, Journal of Geophysical Research: Oceans, 117(C6).

Asplin, M. G., R. Scharien, B. Else, S. Howell, D. G. Barber, T. Papakyriakou, and S. Prinsenberg (2014), Implications of fractured Arctic perennial ice cover on thermodynamic and dynamic sea ice processes, Journal of Geophysical Research: Oceans, 119(4), 2327-2343, doi:10.1002/2013JC009557.

Behroozi, F., J. Smith, and W. Even (2010), Stokes' dream: Measurement of fluid viscosity from the attenuation of capillary waves, American Journal of Physics, 78(11), 1165-1169.

Bidlot, J., S. Keeley, and K. Mogensen (2014), Towards the inclusion of Sea Ice Attenuation in an Operational Wave Model, paper presented at 22nd IAHR International Symposium on Ice, Singapore.

Booij, N., R. C. Ris, and L. H. Holthuijsen (1999), A third-generation wave model for coastal regions: 1. Model description and validation, Journal of Geophysical Research: Oceans, 104(C4), 7649-7666.

Borge, J. C. N., K. Reichert, and J. Dittmer (1999), Use of nautical radar as a wave monitoring instrument, Coastal Engineering, 37(3–4), 331-342, doi:10.1016/S0378-3839(99)00032-0.

Broström, G. and K. Christensen (2008), Waves in sea ice, J. Phys. Oceanogr., 31, 1498-1516.

Campbell, A. J., A. J. Bechle, and C. H. Wu (2014), Observations of surface waves interacting with ice using stereo imaging, Journal of Geophysical Research: Oceans, 119(6), 3266-3284, doi:10.1002/2014JC009894.

Cavaleri, L., J. -. G. M. Alves, F. Ardhuin, A. V. Babanin, M. L. Banner, K. Belibassakis, M. Benoit, M. A. Donelan, M. A. Donelan, J. Groenweg, T. H. C. Herbers, P. A. Hwang, P. A. E. M. Janssen, T. T. Janssen, I. V. Lavrenov, R. Magne, J. Monbaliu, M. Onorato, V. Polnikov, D. Resio, W. E. Rogers, A. Sheremet, J. McKee Smith, H. L. Tolman, G. van Vledder, J. Wolf, and I. R. Young (2007), Wave Modelling – The State of the Art, Prog. Oceanogr., 75(4), 603-674, doi:10.1016/j.pocean.2007.05.005.

Collins III, C. O., W. E. Rogers, A. Marchenko, and A. V. Babanin (2015), In Situ Measurements of an Energetic Wave Event in the Arctic Marginal Ice Zone, Geophys. Res. Lett., 42.6, 1863-1870 doi:10.1002/2015GL063063.

Collins III, C. O., W. E. Rogers, & B. Lund, (2016) The Dispersion of Wind Generated Ocean Surface Waves in Ice Covered Seas, (manuscript in progress for Ocean Dynamics).

Collins III, C. O. (2014), Typhoon generated surface gravity waves measured by NOMAD-type buoys, University of Miami, 337 pp.

Crary, A. P., R. Cotell, and J. Oliver (1952), Geophysical studies in the Beaufort Sea, 1951, Eos, Transactions American Geophysical Union, 33(2), 211-216.

Crocker, G. and P. Wadhams (1988), Observations of wind-generated waves in Antarctic fast ice, J. Phys. Oceanogr., 18(9), 1292-1299.

De Carolis, G., and D. Desiderio (2002), Dispersion and attenuation of gravity waves in ice: a two-layer viscous fluid model with experimental data validation, Physical Letters A, 305, 399-412.

Doble, M. J. and J. Bidlot (2013), Wave buoy measurements at the Antarctic sea ice edge compared with an enhanced ECMWF WAM: Progress towards global waves-in-ice modelling, Ocean Modelling, 70, 166-173.

Dumont, D., A. Kohout, and L. Bertino (2011), A wave-based model for the marginal ice zone including a floe breaking parameterization, Journal of Geophysical Research: Oceans (1978–2012), 116(C4).

Fakidov, I. (1934), Vibrations of the Ice-Cap of Polar Seas, Nature, 134, 536-537.

Fox, C. and T. G. Haskell (2001), Ocean wave speed in the Antarctic marginal ice zone, Annals of Glaciology, 33(1), 350-354.

Fox, C. and V. A. Squire (1994), On the oblique reflexion and transmission of ocean waves at shore fast sea ice, Philosophical Transactions of the Royal Society of London.Series A: Physical and Engineering Sciences, 347(1682), 185-218.

Frankenstein, G. and R. Garner (1967), Equations for determining the brine volume of sea ice from-0.5 C to-22.9 C, J. Glaciol., 6, 943-944.

Frankenstein, S., S. Loset, and H. H. Shen (2001), Wave-ice interactions in Barents Sea marginal ice zone, J. Cold Regions Eng., 15(2), 91-102.

Frannson, L. (2009), Ice Handbook for Engineers, Lule a University of Technology.

Hasselmann, K., T. P. Barnett, E. Bouws, H. Carlson, D. E. Cartwright, K. Enke, J. A. Ewing, H. Gienapp, D. E. Hasselmann, P. Kruseman, A. Meerburg, P. Mller, D. J. Olbers, K. Richter, W. Sell, and H. Walden (1973), Measurements of wind-wave growth and swell decay during the Joint North Sea Wave Project (JONSWAP), Ergnzungsheft zur Deutschen Hydrographischen Zeitschrift Reihe, 8(12), 95.

Hayes, D. R., A. Jenkins, and S. McPhail (2007), Autonomous Underwater Vehicle Measurements of Surface Wave Decay and Directional Spectra in the Marginal Sea Ice Zone*, J. Phys. Oceanogr., 37(1), 71-83.

Herman, A. (2010), Sea-ice floe-size distribution in the context of spontaneous scaling emergence in stochastic systems, Physical Review E, 81(6), 066123.

Holthuijsen, L. H. (2007), Waves in oceanic and coastal waters, Cambridge University Press.

Horvat, C. and E. Tziperman (2015), A prognostic model of the sea ice floe size and thickness distribution. The Cryosphere.

Hunke, E. C., W. H. Lipscomb, and A. K. Turner (2010), CICE: the Los Alamos Sea Ice Model Documentation and Software User's Manual Version 4.1 LA-CC-06-012, T-3 Fluid Dynamics Group, Los Alamos National Laboratory.

Hunkins, K. (1962), Waves on the Arctic Ocean, Journal of Geophysical Research, 67(6), 2477-2489, doi:10.1029/JZ067i006p02477.

Keller, J. B. (1998), Gravity waves on ice-covered water, Journal of Geophysical Research: Oceans, 103(C4), 7663-7669.

Kinsman, B. (1965), Wind waves, their generation and propagation on the ocean surface, Prentice-Hall, Englewood Cliffs, N.J.

Kohout, A. and M. Meylan (2008), An elastic plate model for wave attenuation and ice floe breaking in the marginal ice zone, Journal of Geophysical Research: Oceans (1978–2012), 113(C9).

Kohout, A. L., B. Penrose, S. Penrose, and M. J. Williams (2015), A device for measuring wave-induced motion of ice floes in the Antarctic marginal ice zone, Annals of Glaciology, 56(69), 415-424.

Kohout, A. L., M. Williams, S. Dean, and M. H. Meylan (2014), Storm-induced sea-ice breakup and the implications for ice extent, Nature, 509(7502), 604-607.

Kohout, A., M. Williams, T. Toyota, J. Lieser, and J. Hutchings (2015), In situ observations of wave-induced sea ice breakup, Deep Sea Research Part II: Topical Studies in Oceanography.

Krupnik, I. and W. U. Weyapuk Jr (2010), Qanuq Ilitaavut:"How We Learned What We Know"(Wales Inupiaq Sea Ice Dictionary), in SIKU: Knowing Our Ice, , edited by Anonymous , pp. 321-354, Springer.

Langhorne, P. J., V. A. Squire, C. Fox, and T. G. Haskell (1998), Break-up of sea ice by ocean waves, Annals of Glaciology, 27, 438-442.

LeSchack, L. A. and R. A. Haubrich (1964), Observations of waves on an ice-covered ocean, Journal of Geophysical Research, 69(18), 3815-3821.

Li, J., A. L. Kohout, and H. H. Shen (2015), Comparison of wave propagation through ice covers in calm and storm conditions, Geophys. Res. Lett., 42(14), 5935-5941.

Liu, A. K., B. Holt, and P. W. Vachon (1991), Wave propagation in the marginal ice zone: Model predictions and comparisons with buoy and synthetic aperture radar data, Journal of Geophysical Research: Oceans, 96(C3), 4605-4621.

Liu, A. K. and E. Mollo-Christensen (1988), Wave propagation in a solid ice pack, J. Phys. Oceanogr., 18(11), 1702-1712.

Lund, B., C. O. Collins, H. C. Graber, E. Terrill, and T. H. Herbers (2014), Marine radar ocean wave retrieval's dependency on range and azimuth, Ocean Dynamics, 64(7), 999-1018.

Lund, B., H. C. Graber, K. Hessner, and N. J. Williams (2015), On Shipboard Marine X-Band Radar Near-Surface Current ''Calibration'', J. Atmos. Ocean. Technol., 32(10), 1928-1944.

Marchenko, A., E. Karulin, P. Chistyakov, D. Sodhi, M. Karulina, and A. Sakharov (2014), Three dimensional fracture effects in tests with cantilever and fixed ends beams, paper presented at 22st IAHR International Symposium on Ice, Singapore.

Marko, J. R. (2003), Observations and analyses of an intense waves-in-ice event in the Sea of Okhotsk, Journal of Geophysical Research: Oceans, 108(C9).

McKenna, R. and G. Crocker (1992), Ice-floe collisions interpreted from acceleration data during LIMEX '89, Atmosphere-Ocean, 30(2), 246-269.

Meylan, M. H., L. G. Bennetts, and A. L. Kohout (2014), In situ measurements and analysis of ocean waves in the Antarctic marginal ice zone, Geophys. Res. Lett., 41(14), 5046-5051.

Mosig, J. E., F. Montiel, and V. A. Squire (2015), Comparison of viscoelastic-type models for ocean wave attenuation in ice-covered seas, Journal of Geophysical Research: Oceans, 120(9), 6072-6090.

Perovich, D. K. and K. F. Jones (2014), The seasonal evolution of sea ice floe size distribution, Journal of Geophysical Research: Oceans, 119(12), 8767-8777.

Polnikov, V.G. and I.V. Lavrenov (2007), Calculation of the nonlinear energy transfer through the wave spectrum at the sea surface covered with broken ice. Oceanology, 47(3), 334-343.

Robin, G. d. Q. (1963), Wave propagation through fields of pack ice, Philosophical Transactions for the Royal Society of London. Series A, Mathematical and Physical Sciences, 313-339.

Robinson, N. and S. Palmer (1990), A modal analysis of a rectangular plate floating on an incompressible liquid, J. Sound Vibrat., 142(3), 453-460.

Rogers, W. E., A. V. Babanin, and D. W. Wang (2012), Observation-consistent input and whitecapping dissipation in a model for wind-generated surface waves: Description and simple calculations, J. Atmos. Ocean. Technol., 29(9), 1329-1346.

Rogers, W. E. and G. P. Van Vledder (2013), Frequency width in predictions of windsea spectra and the role of the nonlinear solver, Ocean Modelling, 70, 52-61.

Rogers, W. E. and M. D. Orzech (2013), *Implementation and testing of ice and mud source functions in WAVEWATCH III®*, in , NRL/MR/7320–13-9462.

Rogers, W. E. and S. S. Zieger (2014), S_{ice}: Damping by sea ice, in User manual and system documentation of WAVEWATCH III(R) version 4.18b, , edited by H. L. Tolman, pp. 60-61, College Park, MD, Tech. Note, MMAB Contribution 316 NOAA/NWS.

Rothrock, D. and A. Thorndike (1984), Measuring the sea ice floe size distribution, Journal of Geophysical Research: Oceans (1978–2012), 89(C4), 6477-6486.

Rottier, P. J. (1992), Floe pair interaction event rates in the marginal ice zone, Journal of Geophysical Research: Oceans (1978–2012), 97(C6), 9391-9400.

Sakai, S. and K. Hanai (2002), Empirical formula of dispersion relation of waves in sea ice, paper presented at Ice in the environment: Proceedings of the 16th IAHR International Symposium on Ice.

Sinnett, G. and F. Feddersen (2014), The surf zone heat budget: The effect of wave heating, Geophys. Res. Lett., 41(20), 7217-7226.

Skene, D., L. Bennetts, M. Meylan, and A. Toffoli (2015), Modelling water wave overwash of a thin floating plate, J. Fluid Mech., 777, R3.

Steele, M. (1992), Sea ice melting and floe geometry in a simple ice-ocean model, Journal of Geophysical Research: Oceans (1978–2012), 97(C11), 17729-17738.

Strong, C., & I. G. Rigor (2013), Arctic marginal ice zone trending wider in summer and narrower in winter. Geophysical Research Letters, 40(18), 4864-4868.

Squire, V. A. (1993), A comparison of the mass-loading and elastic plate models of an ice field, Cold Reg. Sci. Technol., 21(3), 219-229.

Squire, V. A. (2007), Of ocean waves and sea-ice revisited, Cold Reg. Sci. Technol., 49(2), 110-133.

Squire, V. A. and F. Montiel (2015), Hydroelastic perspectives of ocean wave/sea ice connectivity I, paper presented at Proceedings of the 7th International Conference on Hydroelasticity in Marine Technology, Split, Croatia.

Squire, V. A. and S. C. Moore (1980), Direct measurement of the attenuation of ocean waves by pack ice, 365-368, doi:doi:10.1038/283365a0.

Tayfun, M. A. and F. Fedele (2007), Wave-height distributions and nonlinear effects, Ocean Eng., 34(11), 1631-1649.

Thomson, J., V. Squire, S. Ackley, E. Rogers, A. Babanin, P. Guest, T. Maksym, P. Wadhams, S. Stammerjohn, C. Fairall, O. Persson, M. Doble, H. Graber, H. Shen, J. Gemmrich, S. Lehner, B. Holt, T. Williams, M. Meylan, and J. Bidlot (2013) Sea State and Boundary Layer Physics of the Emerging Arctic Ocean. Technical Report. APL-UW TR1306, Applied Physics Laboratory, University of Washington, Seattle, Washington.

Thomson, J. and W. E. Rogers (2014), Swell and sea in the emerging Arctic Ocean, Geophys. Res. Lett., 41(9), 3136-3140, doi:10.1002/2014GL059983.

Thorndike, A., D. Rothrock, G. Maykut, and R. Colony (1975), The thickness distribution of sea ice, Journal of Geophysical Research, 80(33), 4501-4513.

Timco, G. W. and W. F. Weeks (2010), A review of the engineering properties of sea ice, Cold Reg. Sci. Technol., 60(2), 107-129, doi:http://dx.doi.org/10.1016/j.coldregions.2009.10.003.

Toffoli, A., L. G. Bennetts, M. H. Meylan, C. Cavaliere, A. Alberello, J. Elsnab, and J. P. Monty (2015), Sea ice floes dissipate the energy of steep ocean waves, arXiv preprint arXiv:1502.06040.

Toffoli, A., T. Waseda, H. Houtani, L. Cavaleri, D. Greaves, and M. Onorato (2015), Rogue waves in opposing currents: an experimental study on deterministic and stochastic wave trains, J. Fluid Mech., 769, 277-297.

Tolman, H. L. (1991), A third-generation model for wind waves on slowly varying, unsteady, and inhomogeneous depths and currents, Journal of Physical Oceanography, 21(6), 782-797.

Tolman, H. L. (2003), Treatment of unresolved islands and ice in wind wave models, Ocean Modelling, 5(3), 219-231.

Tolman, H.L. (2013), A Generalized Multiple Discrete Interaction Approximation for resonant four-wave interactions in wind wave models, Ocean Modelling, vol. 70, 11-24, 10.1016/j.ocemod.2013.02.005.

Tolman, H. L. and the WAVEWATCH III® Development Group (2014), User Manual and System Documentation of WAVEWATCH III® version 4.18, in , 316, NOAA/NWS/NCEP/MMAB.

Toyota, T., C. Haas, and T. Tamura (2011), Size distribution and shape properties of relatively small sea-ice floes in the Antarctic marginal ice zone in late winter, Deep Sea Research Part II: Topical Studies in Oceanography, 58(9), 1182-1193.

Toyota, T., S. Takatsuji, and M. Nakayama (2006), Characteristics of sea ice floe size distribution in the seasonal ice zone, Geophys. Res. Lett., 33(2).

Vaudrey, K. (1977) Ice engineering-study of related properties of floating sea-ice sheets and summary of elastic and viscoelastic analyses. No. CEL-TR-860, Civil Engineering Lab (Navy), Port Hueneme, CA.

Wadhams, P. (1972), Measurement of wave attenuation in pack ice by inverted echo sounding, paper presented at Sea Ice. In Karlsson, T., editor, Sea Ice. Proceedings of an International Conference, pages 255-260. National Research Council, Reykjavik, Iceland.

Wadhams, P. (1973), Attenuation of swell by sea ice, Journal of Geophysical Research, 78(18), 3552-3563.

Wadhams, P. (1975), Airborne laser profiling of swell in an open ice field, Journal of Geophysical Research, 80(33), 4520-4528.

Wadhams, P. (1978), Wave decay in the marginal ice zone measured from a submarine, Deep-Sea Res., 25, 23-40.

Wadhams, P. (1981), The ice cover in the Greenland and Norwegian Seas, Rev. Geophys., 19(3), 345-393.

Wadhams, P. (2000), Ice in the Ocean, CRC Press.

Wadhams, P. and B. Holt (1991), Waves in frazil and pancake ice and their detection in Seasat synthetic aperture radar imagery, Journal of Geophysical Research: Oceans, 96(C5), 8835-8852.

Wadhams, P., V. A. Squire, J. A. Ewing, and R. Pascal (1986), The effect of the marginal ice zone on the directional wave spectrum of the ocean, J. Phys. Oceanogr., 16(2), 358-376.

Wadhams, P., V. A. Squire, D. J. Goodman, A. M. Cowan, and S. C. Moore (1988), The attenuation rates of ocean waves in the marginal ice zone, Journal of Geophysical Research: Oceans, 93(C6), 6799-6818.

Wang, R. and H. H. Shen (2010), Gravity waves propagating into an ice-covered ocean: A viscoelastic model, Journal of Geophysical Research: Oceans, 115(C6).

Weitz, Mortimer, and Joseph B. Keller (1950), Reflection of water waves from floating ice in water of finite depth, Communications on Pure and Applied Mathematics, 3.3: 305-318.

Williams, T. D., L. G. Bennetts, V. A. Squire, D. Dumont, and L. Bertino (2013a), Wave–ice interactions in the marginal ice zone. Part 1: Theoretical foundations, Ocean Modelling, 71, 81-91.

Williams, T. D., L. G. Bennetts, V. A. Squire, D. Dumont, and L. Bertino (2013b), Wave–ice interactions in the marginal ice zone. Part 2: Numerical implementation and sensitivity studies along 1D transects of the ocean surface, Ocean Modelling, 71, 92-101.

Young, I. R., W. Rosenthal, and F. Ziemer (1985), A three-dimensional analysis of marine radar images for the determination of ocean wave directionality and surface currents, Journal of Geophysical Research: Oceans, 90(C1), 1049-1059, doi:10.1029/JC090iC01p01049.

Young, I. and G. P. Van Vledder (1993), A review of the central role of nonlinear interactions in wind-wave evolution, Philosophical Transactions of the Royal Society of London A: Mathematical, Physical and Engineering Sciences, 342(1666), 505-524.

Zhang, J., A. Schweiger, M. Steele, and H. Stern (2015), Sea ice floe size distribution in the marginal ice zone: Theory and numerical experiments, Journal of Geophysical Research: Oceans.

Zhao, X. and H. H. Shen (2015), Ocean wave transmission and reflection by viscoelastic ice covers, Ocean Modelling.

Zhao, X., H. H. Shen, and S. Cheng (2015), Modeling ocean wave propagation under sea ice covers, Acta Mechanica Sinica, 31(1), 1-15.